



**Politecnico  
di Torino**

## Politecnico di Torino

Corso di Laurea Magistrale in Ingegneria per l'Ambiente e il Territorio

A.A. 2022/2023

Sessione di laurea: novembre-dicembre 2022

### “Flow and heat transport modelling of an open-loop shallow geothermal system”

**Relatori:**

Prof. Ing. Alessandro Casasso

**Correlatore:**

Dott. Geol. Marco Orsi

**Candidato:**

Mattia Agrusti  
(matr. 279010)







# TABLE OF CONTENTS

|  |    |
|--|----|
| ABSTRACT   | 3  |
| 1 INTRODUCTION                                   | 4  |
| 1.1 Shallow geothermal systems                   | 4  |
| 1.2 Closed-loop shallow geothermal systems       | 6  |
| 1.3 Open-loop shallow geothermal systems         | 8  |
| 1.3.1 Installation                               | 9  |
| 1.3.2 Design of GWHPs                            | 11 |
| 1.3.3 Thermal and Hydraulic recycling            | 11 |
| 1.4 Heat Pumps                                   | 12 |
| 1.4.1 Parameters                                 | 14 |
| 2 CASE STUDY                                     | 15 |
| 2.1 The real estate project “Parco delle Favole” | 15 |
| 2.2 Hydrogeological setup                        | 16 |
| 2.3 The open-loop geothermal system              | 18 |
| 2.3.1 The HVAC system                            | 18 |
| 2.3.2 The wells field                            | 22 |
| 2.4 Hydraulic characterisation of the aquifer    | 25 |
| 2.4.1 Step drawdown test                         | 26 |
| 2.4.2 Long-term pumping test                     | 28 |
| 2.4.3 Lefranc test                               | 29 |
| 2.4.4 Reinjection test                           | 30 |
| 2.4.5 Summary of the results                     | 30 |
| 3 MONITORING SYSTEM                              | 32 |
| 3.1 Groundwater monitoring                       | 32 |
| 3.1.1 Monitoring network installed               | 32 |
| 3.1.2 Analysis of monitoring data                | 36 |
| 3.2 Flow rate monitoring system                  | 37 |

|       |  |    |
|-------|--|----|
| 4     | SUBSURFACE FLOW AND HEAT TRANSPORT MODELLING | 40 |
| 4.1   | Flow and heat transport in porous media      | 40 |
| 4.2   | Development of the numerical model           | 42 |
| 4.2.1 | Conceptual model                             | 42 |
| 4.2.2 | The modelling domain                         | 42 |
| 4.2.3 | Modelling setup                              | 46 |
| 4.3   | Results and discussion                       | 51 |
| 5     | CONCLUSIONS                                  | 61 |
|       | REFERENCES                                   | 62 |

## ABSTRACT

Shallow geothermal systems are being increasingly adopted for heating and cooling of buildings due to their low maintenance costs and their low carbon footprint. However, the exploitation of shallow subsurface for geothermal purposes must be carefully evaluated to avoid overexploitation and negative impacts on existing installations.

This thesis deals with the assessment of the thermal impact of a groundwater heat pump to be installed for a block of flats in Milan, where a large number of shallow geothermal systems is already present. The plant will cover the heating, cooling, and domestic hot water needs of 100 housing units, and it is composed of two abstraction wells and three reinjection wells, screened in the shallow unconfined aquifer.

Existing geological and hydrogeological information was analysed to derive the conceptual model, on which a numerical flow and heat transport model was built with the finite-element modelling code FEFLOW 7.5. The operation of the plant was simulated considering thermal loads derived from dedicated design reports, i.e., with monthly time steps. As reported in several studies in the literature, such a time resolution allows for a precise reconstruction of the thermal impact of the plant, which is the main purpose of this study. The results of numerical simulation prove that the plant is not expected to exert any appraisable thermal impact on existing installations and that no thermal recycling is expected. Results also allowed to draw some preliminary conclusions on the sustainable density of open-loop shallow geothermal systems in the area where the plant is located.

# 1 INTRODUCTION

The need to reduce greenhouse gas (GHG) emissions, along with the periodic energy crises that occurred in the last 50 years, has fostered the development of renewable energy sources (RES).

According to the Italian Energy Agency ENEA [1], the energy demand of Italy in 2019 was equal to 155.4 MTOE, of which 19% was covered by RES. Civil uses (especially space heating) absorb 41.1% of the overall primary energy demand, followed by the transport sector (29.8%) and industry (20.7%). These figures confirm the importance of the residential sector in the decarbonisation of the Italian energy system. So far, most of the RES production in this sector was achieved with wood biomass; however, the concerns for air quality suggest that other sources, such as heat pumps, must be considered for a further expansion of RES use for space heating. For this reason, the EU Roadmap considers heat pumps as the main technologies to achieve the of 100% renewable heating network. Heat can use air or ground as heat sources respectively called Air Source (ASHP) and Ground Source Heat Pumps (GSHPs), able to achieve significant economic saving [2]. GSHP systems exploit geothermal energy comes from the internal geothermal flow.

This thesis deals with an open loop system for heating and cooling of a block of flats in Milan purposes and is structured as follows. The remainder of this section presents basic information on open-loop shallow geothermal systems. Section 2 analyses the case study from hydrogeological point of view, deepening the study of aquifer parameters. Section 3 deals with the development of a temperature, flow, and groundwater level monitoring system for the plant, with the analysis of the first monitoring data available. Section 4 focuses on the simulation of the plant operation through subsurface flow and heat transport modelling with, FEFLOW. Section 5 summarizes the results of the work and the conclusions that can be drawn from them.

## 1.1 Shallow geothermal systems

Geothermal energy is the heat that is generated and transferred in the subsurface in different forms (hot rocks, vapours, hot water, water at ambient temperatures) and at different depths (from a few meters to a few km from the ground surface). Geothermal resources are classified, based on the temperature of fluids, in three main typologies [3]:

- high enthalpy: fluid at temperature exceeding 150°C, mainly exploited for electricity purposes;
- medium enthalpy: temperatures between 90 and 150°C, for direct heat uses or for electricity production;
- low enthalpy: below 90°C, for heating uses only, both direct or (for ambient temperatures) with heat pumps (ground sources or geothermal heat pumps).



Geothermal resources at different temperatures therefore have different uses, as represented in Fig. 1. Among them, geothermal heat pumps (also known as Ground Source Heat Pumps, GSHPs) are based on the use of a heat pump to transfer thermal energy from the subsoil to the building air conditioning plant and are divided in two main categories (Fig.2):

- closed-loop: based on the circulation of a heat carrier fluid in a closed pipe loop buried into the ground (Borehole Heat Exchanger, BHE);
- open-loop, based on thermal exchange on groundwater (Ground Water Heat Pump, GWHP).

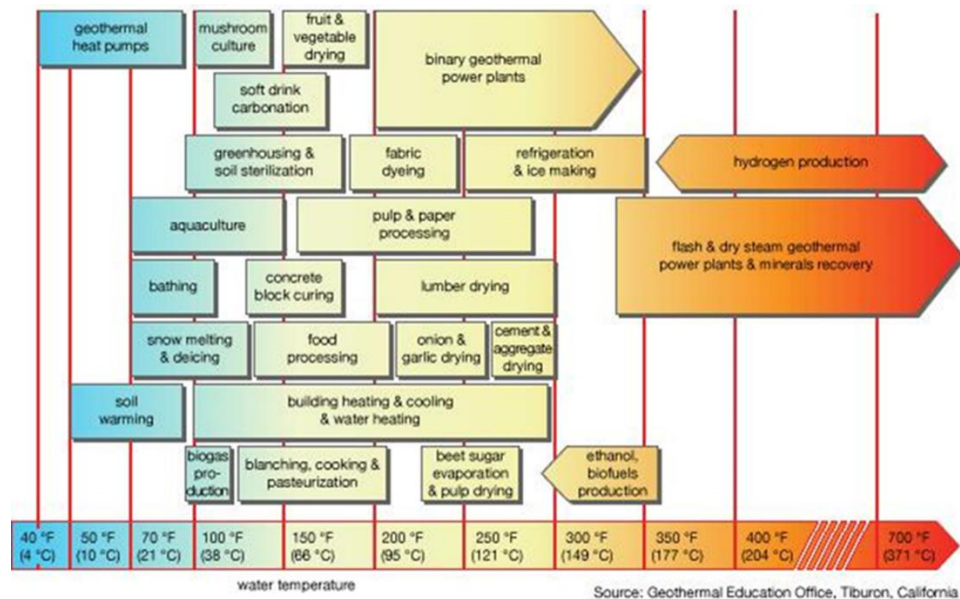


Fig. 1. Representation of possible uses of geothermal energy at different temperatures.

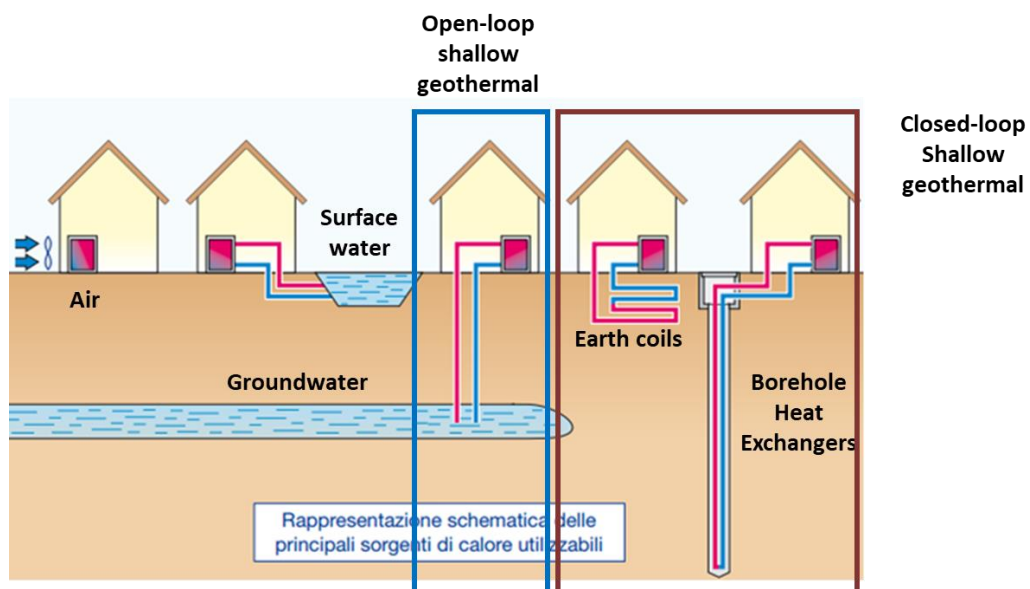


Fig. 2. Different types of heat pumps. Adapted from [4].

A traditional low enthalpy geothermal system like Ground Source Heat Pump (GSHP) is composed by:

- heat exchanger, distinguished in closed-loop Borehole Heat Exchange, (BHE) and open-loop system (Ground Water Heat Pump, GWHP);
- Heat Pump (HP);
- air conditioning terminal, so the distribution plant.

In the following paragraphs it will be analysed all components above, explaining a part of different existing available solutions, focusing more attention on open-loop system, object of this thesis.

## 1.2 Closed-loop shallow geothermal systems

In the closed-loop system, the heat exchange is performed by means of hydraulic closed pipes circuit, buried in the ground, through which circulate a heat carrier fluid. The connection between ground and geothermal circuit is performed by grout mixing that allows heat exchange between the borehole and the ground ( $2 \div 2.2 \text{ W/mK}$ ) and at the same time represents a mechanical tube protection. The geothermal grout ensures perfect sealing between pipes and ground; it composed by Portland concrete mixed with bentonite, quartz sand and additives. For its aim, must not be very porous and characterised by low viscosity.

There are three main categories of closed loop plant, which differ for structures and design:

- geothermal piles: the heat transfer is performed by pipes integrated in the foundation ( Fig. 3);
- Shallow Horizontal Collectors (SHC): exploits a shallow heat transfer circuit at depth not higher than three meters. The heat transfer circuit is available in three different configurations, especially coils, linear or geothermal baskets (Fig. 4).
- Borehole Heat Exchanger (BHE): where pipes installed in vertical boreholes and filled with geothermal grout (a mixture of bentonite and concrete). Very diffuse because can be installed almost everywhere, needs low surface compared for example to SHC and is easier to design and manage (Fig. 5).

Closed loop plants are more diffuse compared to open loop systems because can be installed also in that area where can't exploit groundwater and provides easier application procedures.



Fig. 3. Geothermal piles.



Fig. 4. Shallow Horizontal Collectors (SHC).



Fig. 5. Borehole Heat Exchanger (BHE).

### 1.3 Open-loop shallow geothermal systems

In GWHPs the heat exchange is performed between heat pump and extracted groundwater, generally re-injected into the same aquifer. For this reason, the traditional configuration provides design of two or more distinct wells respectively for extracted and injected groundwater.

There are three different types of open loop systems:

- GWHP with re-injection: the extraction and re-injection of water is performed in the same aquifer using two or more wells; more common but maximum attention for the thermal and hydraulic recycling phenomena; the plant is shown in Fig. 6.
- GWHP without reinjection: the extracted water is not injected in in the same aquifer but in a surface water body system near the plant (ex. lake, river...); this is the easier and cheaper way to discharge and, at the same time, avoid phenomena called thermal recycling. However, this application creates a decay of performance and ground water quality;[4]
- standing column well: is realised just one vertical well, by means is performed extraction and injection; cheaper but less used and diffused compared to other configurations, due to complexity of system. The system is shown in Fig. 7.

It will be focused the attention on the GWHP systems with re-injection in the next paragraphs and will be defined all phases concerning installation of components, dimensioning and operating cycle of the plant.

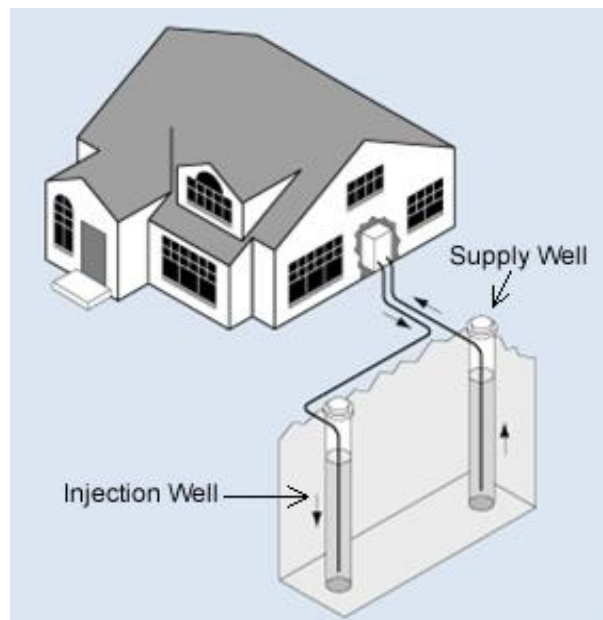


Fig. 6. GWHP with re-injection.

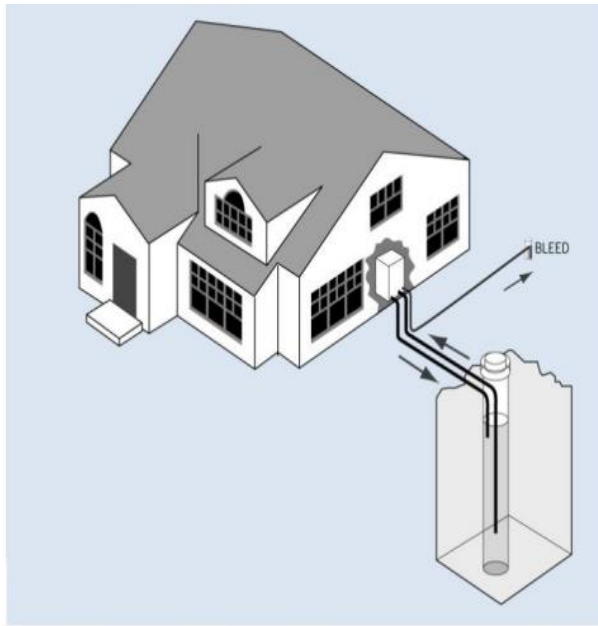


Fig. 7. Standing column well.

### 1.3.1 Installation

How anticipate before, GWHP systems with re-injection predict at least the installation of two wells, extraction well and re-injection well, located in such way that exploit the hydraulic gradient of aquifer and avoid thermal recycling. There are a lot of ways to extract water from the ground and different drilling methods, based on wide range of machines and tools. The most common are resumed as follow:

- percussion method: exploits percussion of a special hammer to drill the soil, repeatedly left dropped, able to realize large diameter wells, more than 1 m. It's not necessary use drilling fluid. Nevertheless, reaches depth not higher than 10-20 m;
- rotary with direct circulation method: the drilling action takes place by rotary movement of the bit fixed to the lower end of the tool; the drilling fluid is pumped through the rotating head inside the drill rods, until it exits at high speed from the cavity of the bit; the fluid and debris then rise along the interspace between the drilling string and the walls of the well and are discharged into the settling tank. The debris settle on the bottom and the mud passes into a second tank to be aspirated by a pump and came back into circulation through the drill string. Technique used for small diameter wells without depth limitations;
- rotary with reverse circulation method: the same principle of rotary drilling but the perforation fluid and debris are aspirated through the cavities in the bit and using the drilling rods as a conduit, they reach the settling tank on the surface. The debris is retained, while the fluid returns by gravity inside the hole. In this case is used for large diameters and deep wells.

- roto-percussion or Downhole (DTH) Hammer: used to drill large, deep holes in hard rock formations or concrete. The DTH is positioned at the end of the drill string, it's screwed to the drill rod which delivers a drilling fluid powering the hammer mechanism. The hammer itself moved by the drilling fluid, hitting the anvil at the back of the drill bit. The drilling fluid exits the DTH at the drill bit, removing all the cuttings and is also responsible for wellbore control. [5]

At the end of drilling operations, can be installed the well. In particular, extraction well is composed by:

- casing, which crosses the unsaturated zone of aquifer;
- screen, effective productive part of the pipe, through flowing water;
- submersible pump and adduction system that links well to heat pump cab.

The pipes, which compose the well, change on the base of the project purposes and the type of subsoil. Especially, can be in PVC, zinc or carbon-bitumen steel and stainless steel. The scheme of system is shown in Fig. 8

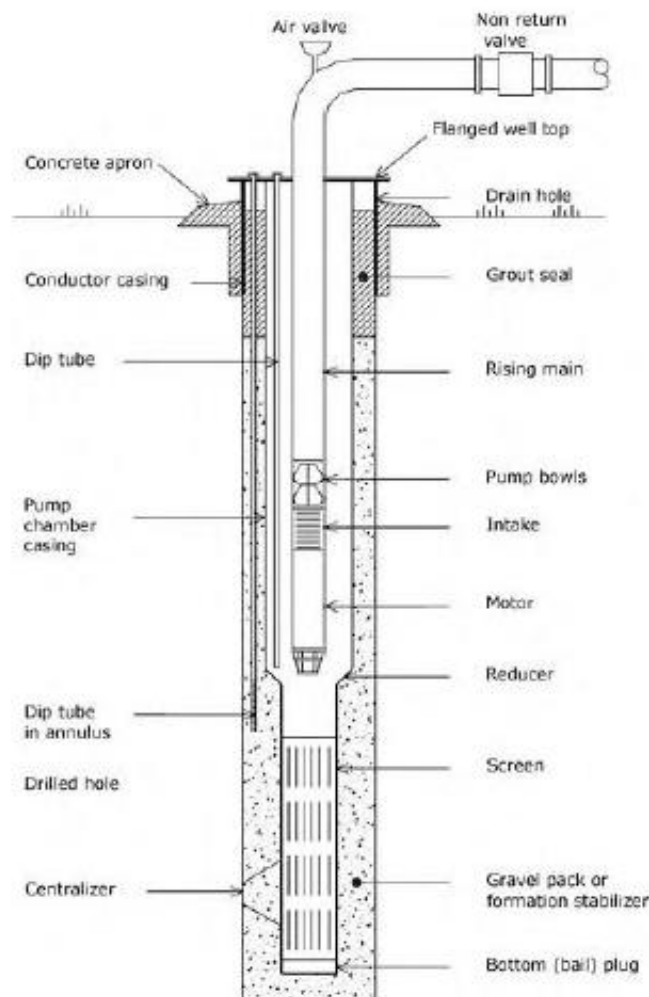


Fig. 8. Extraction well scheme. Source: [6].

### 1.3.2 Design of GWHPs

The design of GWHPs based on a range of factors concerning:

- heating and cooling needs;
- hydraulic properties of the aquifer;
- available site space;
- law requirements.

The thermal power  $P$  [kW] exchanged with groundwater is defined by the following equation:

$$P = (pc)_w Q \Delta T_w \quad \text{Eq. 1}$$

with:

- $Q$  [m<sup>3</sup>/h] is the abstracted flow.
- $\Delta T_w$  [K] is the temperature difference between extracted and injected water.
- $(pc)_w$  is the thermal capacity of water equal to 1.16 kWh/m<sup>3</sup>K.

Notes that different values of  $Q$  and  $\Delta T_w$  give a range of thermal power variation, in particular:

$Q$  is function of hydraulic properties of the aquifer and by law authorizations linked to procedure type thresholds, while  $\Delta T_w$  is function of temperature regulation, variable respect to the analysed area. In open-loop systems with re-injection in the ground,  $\Delta T_w$  must be as contained as possible to avoid microbiological and geothermal alteration of the aquifer system.[4]

### 1.3.3 Thermal and Hydraulic recycling

One of the most relevant phenomena detected in open-loop system is the thermal and hydraulic recycling. This happen when the injection is performed in the capture area of extraction well; in this way the injected water returns to the abstraction well whit a gradual worsening of the performance of the system[4]. For this reason, particular attention must be paid for design of the plant, especially the distance among abstraction and injection well (Fig. 9). Studies prove that in an open-loop system operating at a constant flow rate  $Q$ , thermal recycling occurs if :

$$x = \frac{2Q}{\pi b K i L} > 1 \quad \text{Eq. 2}$$

whit:

- $Q$  [m<sup>3</sup>/d]: hydraulic flow.
- $b$  [m]: aquifer thickness.
- $K$  [m/s]: hydraulic conductivity.
- $L$  [m]: distance between wells.
- $i$  [/]: hydraulic gradient.
- $T$  [m<sup>2</sup>/s]: aquifer transmissivity equal to  $K \cdot b$ .



So, the minimum well distance to avoid thermal recycling is:

$$L > \frac{2Q}{\pi T i} \quad \text{Eq. 3}$$

Others main groundwater issues of GWHPs could be involve the extraction phases; for example, the drawdown effect detected in the well. Similarly, the re-injection could verify a rapidly level rise in the wells, flooding the soil. For this reason, generally, is performed a re-injection test able to evaluate the rise level of groundwater corresponding to a specific injected flow.

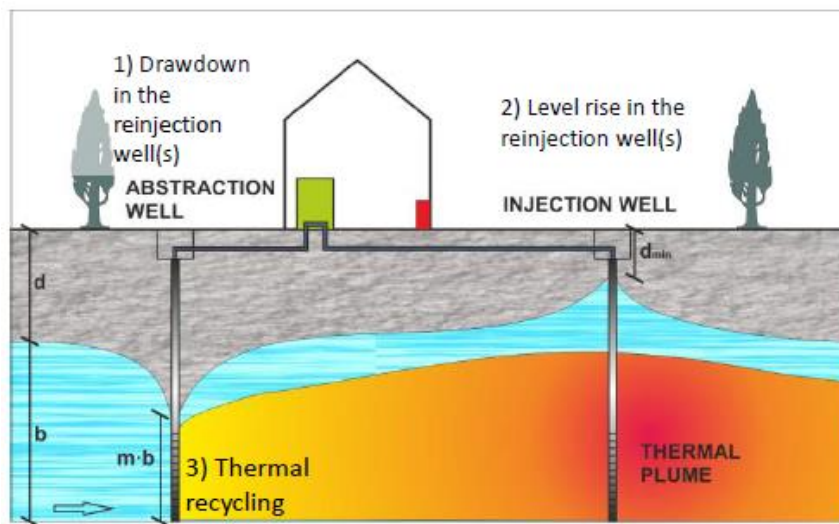


Fig. 9. Thermal Plume GWHP.

## 1.4 Heat Pumps

The Heat Pump is a machine able to transfer heat from a low temperature source to a high temperature sink, exploiting the ability of a refrigerant fluid to absorb and deliver a large amount of heat in the transitions phase. More important underline, consequence of the second principle of thermodynamics, every transformation could not be performed without an external energy input.

HPs are essentially made by closed circuit in which it comes continuously compressed and made to expand a special fluid, called intermediate or refrigerant. With each compression and each expansion, the intermediate fluid steals some heat from the cold fluid and gives it to the hot one. This is a particular fluid that present some specific characteristics:

- high latent heat of vaporization/condensation;
- low evaporation and condensation pressure;
- far below the critical point at the operating temperatures;
- stability and chemical compatibility with the HP materials and lubricant;
- no corrosive, no flammable, no toxic;



- null ozone impact (ODP);
- low-null global warming power (GWP);
- low cost.

Reversing the work cycles, these machines, can be used for cooling purposes and, in this case, are called refrigerant machines.

There are two possible functioning of HP:

- vapour compression (more common), where the increase of pressure is performed by a mechanical compressor;
- absorption, where the compressor is replaced by heat source and a binary fluid, generally aqueous solution of BrLi or NH<sub>3</sub>.

Object of this study, the operating of vapour compression HP based on 4 distinct phases according to the ideal Carnot cycle:

- 1) Evaporation: the refrigerant fluid evaporates suppling heat from outside.
- 2) Compression: the compressor restricts the refrigerant fluid increasing its temperature.
- 3) Condensation: the gaseous refrigerant surrenders heat and thus passing back to the liquid phase.
- 4) Expansion: the pression is reduced, decreasing the temperature of refrigerant that is ready to start again the cycle; the heat pump's scheme is shown in Fig. 10.

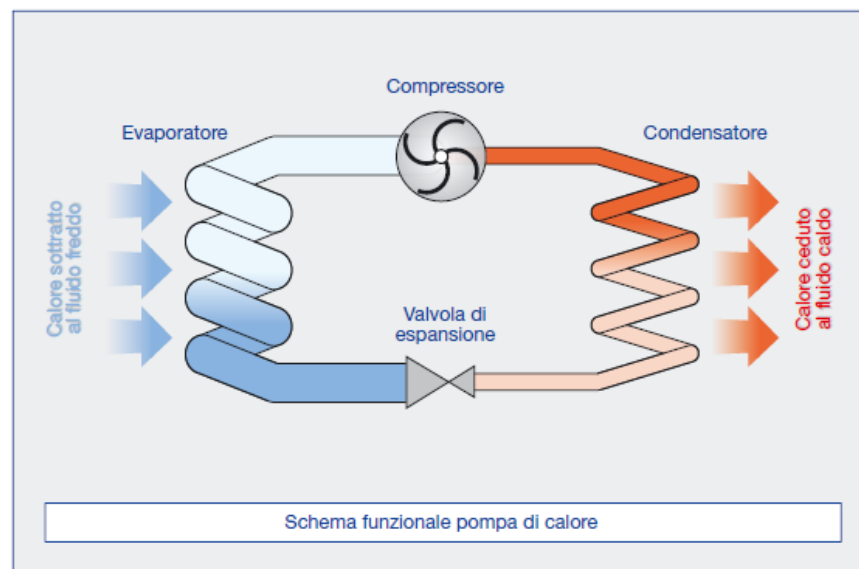


Fig. 10. Heat Pump operating scheme. Source: [7].

In the reality, real Carnot cycle is little more complicated than the ideal one, because there are different intermediate phases (Fig. 11); specifically:

- evaporation is distinct in two phases: an isothermal evaporation (1-2) and a superheating (2-2') recovering heat from the compressor;

- condensation based on three phases: de-superheating phase (3-3'), an isothermal condensation (3'-4) and the last one, an under-cooling of saturated liquid (4-4').

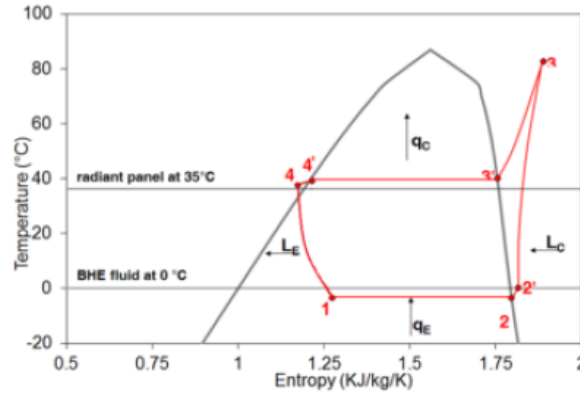


Fig. 11. Real Carnot Cycle.

#### 1.4.1 Parameters

The HP efficiency is expressed by a parameter called coefficient of performance for heating purposes (COP), equal to the ratio between the useful effect of the HP and the work spent by the compressor (Lc). While EER is used for cooling cycle. In the following equations are respectively defined:

$$COP = \frac{q_c}{L_c} = \frac{T_2}{T_2 - T_1} \quad \text{Eq. 4}$$

case of  $T_1 < T_2$ , with:

- $q_c$  is the heat delivered in the condensation phase.

Note that  $T_1$  is the cool source and  $T_2$  the hot source expressed in K.

$$EER = \frac{q_e}{L_c} = \frac{T_1}{T_2 - T_1} \quad \text{Eq. 5}$$

case of  $T_1 > T_2$ , whit:

- $q_e$  is the heat abstracted in the evaporation phase.

The real values of COP and EER are lower than defined one above, because are referred to an ideal cycle Carnot case. For this reason, is possible define a Carnot efficiency parameter equal to:

$$\eta_{Carnot} = \frac{COP_{real}}{COP_{Carnot}} = 0.4 \div 0.5 \quad \text{Eq. 6}$$

## 2 CASE STUDY

### 2.1 The real estate project “Parco delle Favole”

The area of interest, once a contaminated site exploits for industrial purpose, is located between Via Pastro and Via Vignati in Milan, Italy. The project, called “Residenza Parco delle Favole”, has the aim to enhance the area, according to the concept of sustainability and environmental protection. In particular, it bases on the building of 100 housing units, distributed in three buildings (denominates respectively A, B and C) for a maximum of 10 floor, as shown in Fig. 12. Moreover, the total area will be equipped of green spaces (Fig. 13), a gym and child area dedicated. [8]



Fig. 12. Detail of “Residenza Parco delle favole”. Source: Urban File Blog [8].



Fig. 13. Detail of “Residenza Parco delle favole”. Source: Urban File Blog [8].

## 2.2 Hydrogeological setup

The area of Milan is mainly in level, declined from north (140 m asl) to south (102 m asl); the investigated site rises at 135 m asl. From geological point of view the subsoil is composed of a series of sediments, consisting in the deeper part mainly of silts and clays with sands and gravels, while in the upper part there is a wide range of gravels, sands, silts, and clays, as shown in Fig. 14.

The shallow aquifer is composed by gravelly - sandy unit and sandy - gravelly unit defined as follow:

- gravelly - sandy unit, characterized by coarse lithotypes, with clayey slice of limited thickness. The dominant presence of gravel and coarse sand make this layer very permeable; the maximum depth reached is around 40 m from the ground;
- sandy - gravelly unit: very similar grain pack size compared to gravelly-sandy unit with the prevalence of medium and thin sandy fractions, reaching a maximum depth of 100 m in the area of Milan.

The deeper layers are characterized by low permeable natural materials that create a clear separation between shallow aquifer and deeper one; this last, a no permeable horizon, consisting of clay and silts. The present study will be focused on the investigation of shallow aquifer, characterised by an average thickness of 100 m.

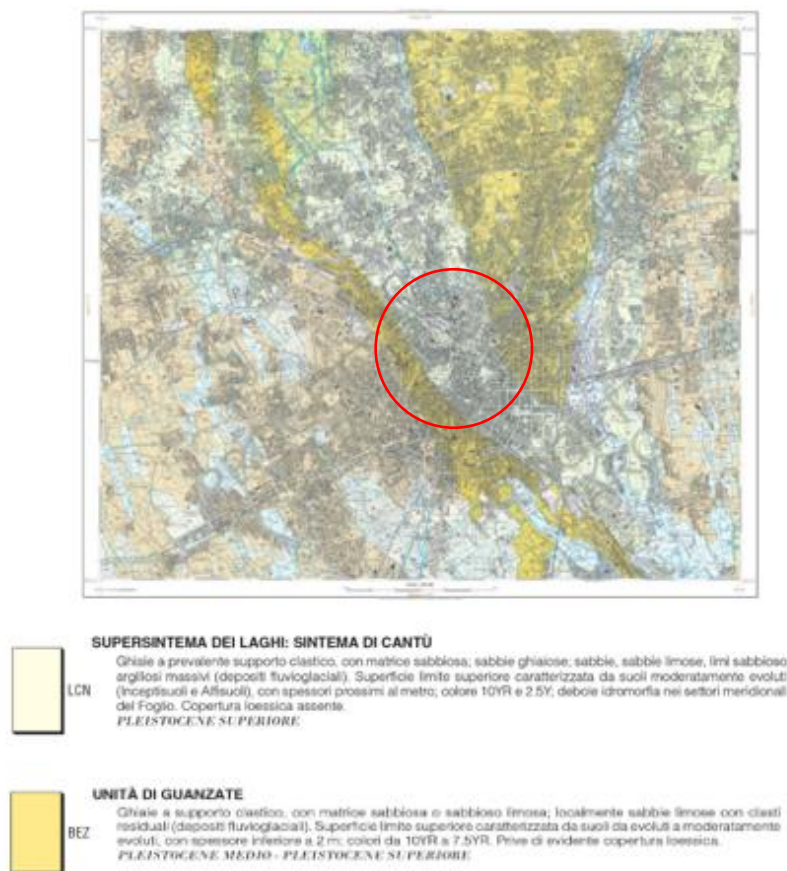


Fig. 14. Carta Geologica Italiana. Foglio 118. Source: [9].



The shallow aquifer, is characterized by transmissivity value 'T' variable between  $5 \cdot 10^{-3} \text{ m}^2/\text{s}$  and  $2 \cdot 10^{-2} \text{ m}^2/\text{s}$ , this last value recorded in the area of Milan [10].

In the following figures (Fig. 15, Fig. 16 and Fig. 17) the representative sections of subsoil of the investigated area.

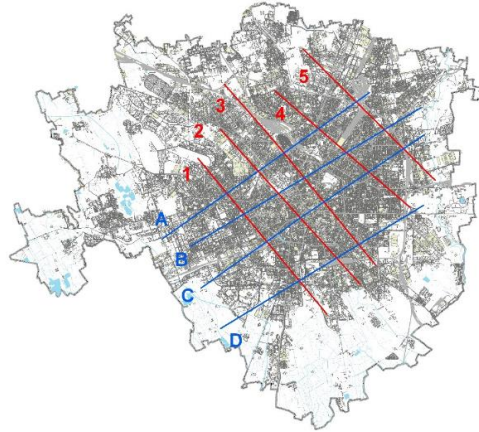


Fig. 15. Hydrogeological section of city of Milan [10].

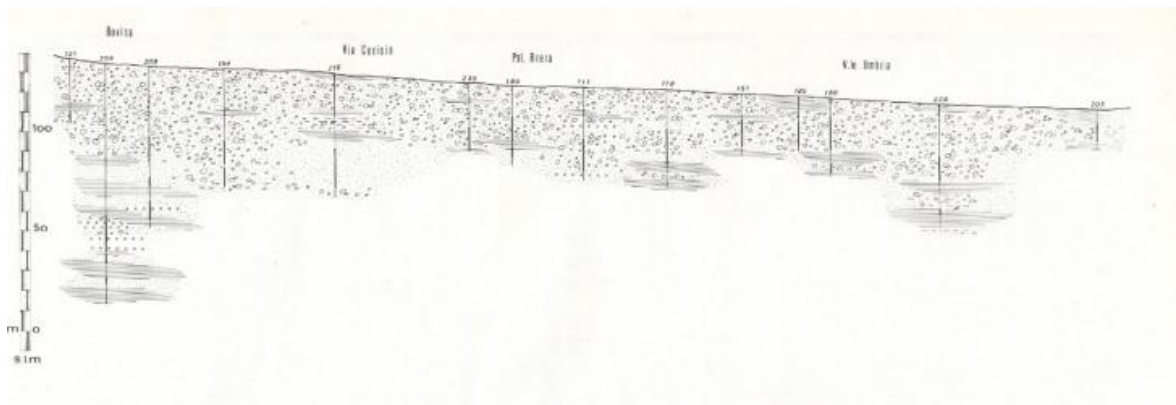


Fig. 16. Hydrogeological section 3. Source: PGT city of Milan [10].

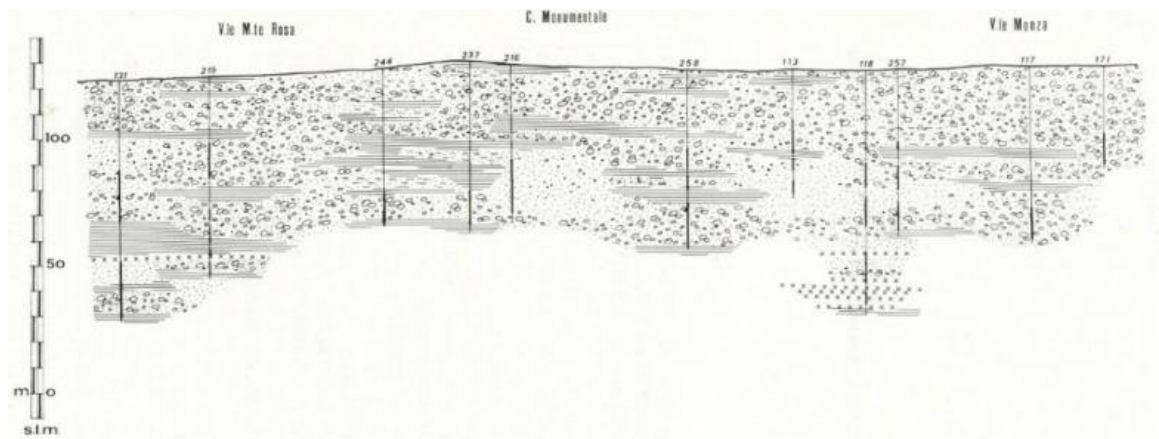


Fig. 17. Hydrogeological section: A. Source: PGT city of Milan [10].

Studies conducted by the municipality of Milan concerning the updating of the PGT (Piano di Governo del Territorio) show how the groundwater flow is directed from North-West to East-South, result obtained thanks to the monitoring network composed by more than 400 wells installed in the area of Milan. The result of monitoring is show in Fig. 18, representation of iso-piezometric curves distribution.

The hydraulic gradient is variable between 1‰ and 0.2‰, result of the extraction activity distributed on the territory. The groundwater lever monitoring, at the same time, shows how its strongly variation zone by zone; in particular, value less than 5 m are detected at the western, southern, and eastern border while at the norther borders the groundwater level is always higher than 10 m, till the middle area of Milan where was recorded level around 15-17 m.

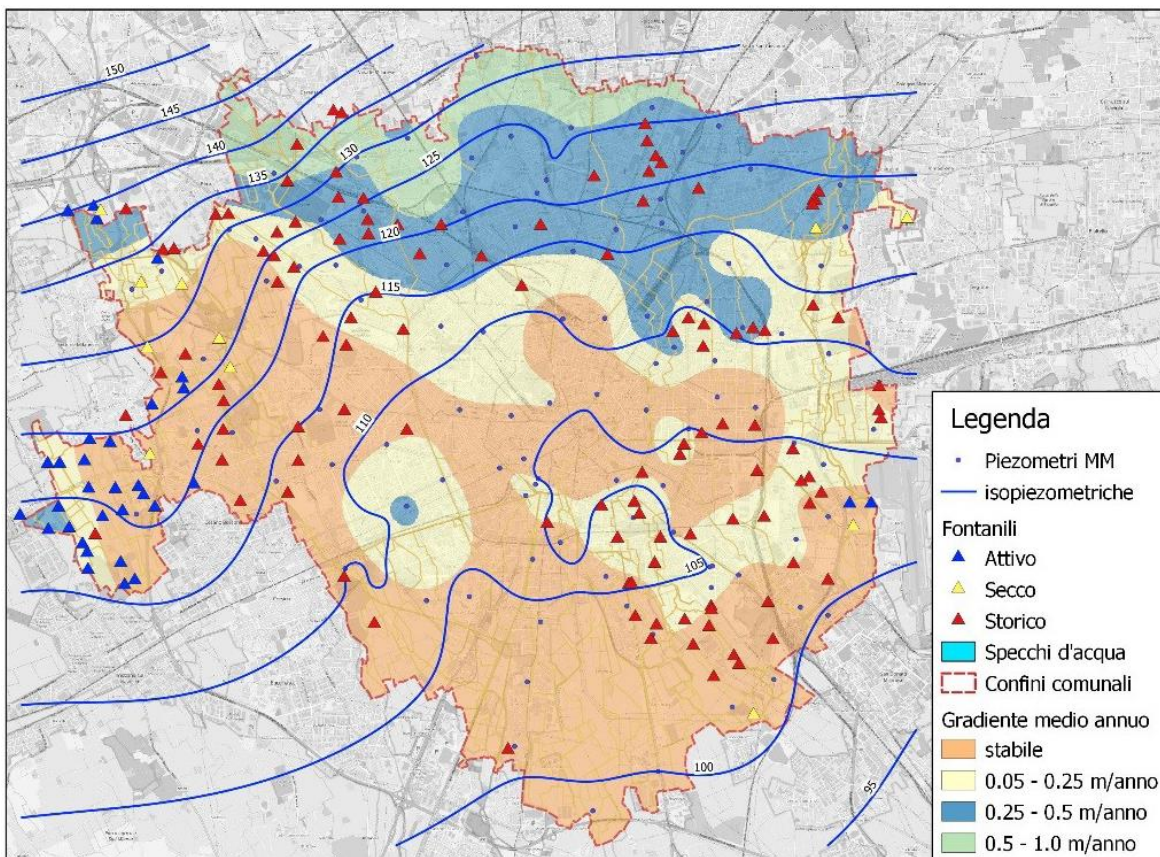


Fig. 18 . Piezometric groundwater level city of Milan. Source: PGT city of Milan [8].

## 2.3 The open-loop geothermal system

### 2.3.1 The HVAC system

The heating ventilation and air conditioning systems (HVACs) are defined as the net of technologies and devices that provide thermal indoor comfort. Generally, used for civil or industrial buildings, can

ensure air quality system and autoregulation of temperature. The HVACs represent a revolution of efficiency energy compact, increasing performance of plant and reducing energy consumptions.

The project of via Pastro has the aim to exploit natural source for cooling and heating purposes and production of sanitary water (DHW). Once pumped groundwater from the extraction wells, this is conducted to the thermal station by a net of pipes. The project provides 3 thermal stations one for each building, inside them are located heat pumps. The plant counts 4 heat pumps, one for the buildings denominates A and B and 2 heat pumps for the building C.

The operating scheme of HP is represented in Fig. 19. The extracted water from the ground is filtered to detain smaller suspended particles. Then, is present a plate heat exchanger, in which happen the exchange between the 2 fluids, followed by heat pump. In particular, considering the project requirements, it was chosen a heat pump marked “Alpha Innotec”, model SWP 691. The operating characteristics of HP are resumed in Tab. 1.

Tab. 1. Operating characteristics of heat pump.

| Model HP  | COP | EER  | Heating power [kW] | Cooling Power [kW] | Adsorbed power [kW] |
|-----------|-----|------|--------------------|--------------------|---------------------|
| SWP - 691 | 4.6 | 5.08 | 92.8               | 81.79              | 16.00               |

Moreover, is included a buffer, a reservoir projected to store thermal energy and be exploited, if necessary, thanks a thermoregulation system.

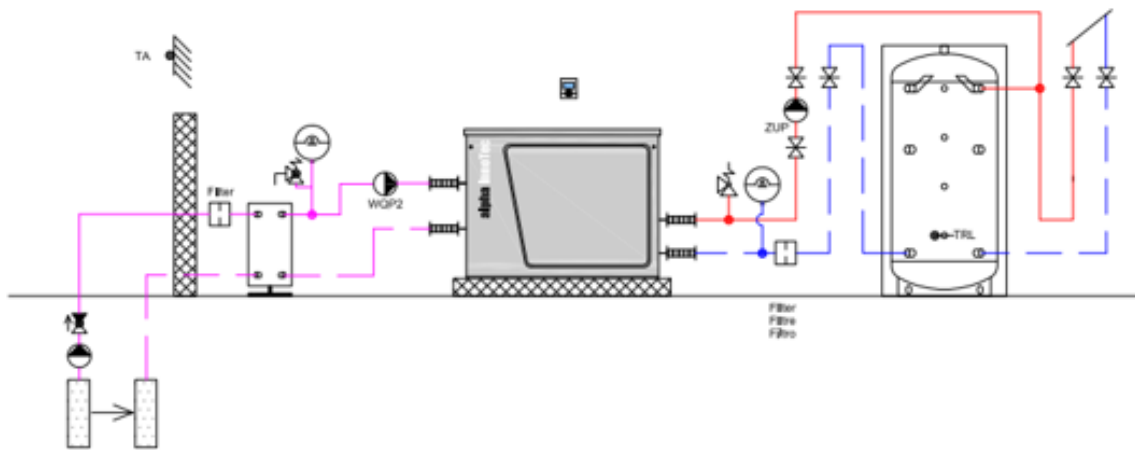


Fig. 19. Thermal station scheme [11].

Defined the thermal station, it was conducted an analysis concerning the needed power for heating, cooling purposes and hot sanitary water for the personal daily hygiene, accessible services installed in the 3 buildings. In Tab. 2, Tab. 3 and Tab. 4 a resume of primary energy needs.

Tab. 2. Heating energy demand for months.

| Period   | Heating energy demand<br>building A [kWh] | Heating energy demand<br>building B [kWh] | Heating energy demand<br>building C [kWh] |
|----------|---|---|---|
| January  | 17045                                     | 19097                                     | 32612                                     |
| February | 9849                                      | 11372                                     | 19080                                     |
| March    | 3865                                      | 4918                                      | 7601                                      |
| April    | 267                                       | 403                                       | 645                                       |
| October  | 1331                                      | 1735                                      | 2645                                      |
| November | 11244                                     | 12717                                     | 21634                                     |
| December | 18534                                     | 20614                                     | 35423                                     |

Tab. 3. Cooling energy demand for months.

| Period    | Cooling energy demand<br>building A [kWh] | Cooling energy demand<br>building B [kWh] | Cooling energy demand<br>building C [kWh] |
|-----------|---|---|---|
| April     | 12  | 8   | 45  |
| May       | 2874                                      | 2594                                      | 5544                                      |
| June      | 9194                                      | 9242                                      | 17135                                     |
| July      | 12162                                     | 12550                                     | 22897                                     |
| August    | 10657                                     | 11057                                     | 20249                                     |
| September | 2337                                      | 1952                                      | 4701                                      |
| October   | 3   | 0   | 3   |

Tab. 4. DHW energy demand for months.

| Time      | DHW energy demand<br>building A [kWh] | DHW energy demand<br>building B [kWh] | DHW energy demand<br>building C [kWh] |
|-----------|---------------------------------------|---------------------------------------|---------------------------------------|
| January   | 5193                                  | 5362                                  | 9293                                  |
| February  | 4365                                  | 4460                                  | 7746                                  |
| March     | 4109                                  | 4086                                  | 7108                                  |
| April     | 3576                                  | 3736                                  | 6532                                  |
| May       | 3865                                  | 3821                                  | 6712                                  |
| June      | 3984                                  | 3840                                  | 6943                                  |
| July      | 4185                                  | 4068                                  | 7359                                  |
| August    | 4323                                  | 4258                                  | 7652                                  |
| September | 4077                                  | 3958                                  | 7056                                  |
| October   | 4462                                  | 448                                   | 47806                                 |
| November  | 4910                                  | 5056                                  | 8792                                  |
| December  | 5245                                  | 5423                                  | 9397                                  |

For each service it was indicated the energy demand. By simply conversion is possible obtain the overage power demand, resumes in Tab. 5



Tab. 5. Power for heating, cooling and DHW purposes.

| Time Interval [d] | Heating power [kW] | Cooling power [kW] | Domestic hot water DHW power [kW] |
|-------------------|--------------------|--------------------|-----------------------------------|
| 0                 | 92.411             | 0                  | 26.677                            |
| 31                | 59.972             | 0                  | 24.659                            |
| 59                | 22.022             | 0                  | 20.569                            |
| 90                | 3.653              | 0                  | 19.228                            |
| 105               | 0.000              | 0.180              | 19.228                            |
| 120               | 0.000              | 14.801             | 19.352                            |
| 151               | 0.000              | 49.404             | 20.510                            |
| 181               | 0.000              | 63.990             | 20.984                            |
| 212               | 0.000              | 56.401             | 21.819                            |
| 243               | 0.000              | 12.486             | 20.960                            |
| 273               | 0.000              | 0.0166             | 23.264                            |
| 288               | 14.872             | 0                  | 21.815                            |
| 304               | 70.025             | 0                  | 26.053                            |
| 334               | 88.179             | 0                  | 26.969                            |
| 365               | 92.411             | 0                  | 26.677                            |

The power request by HP in time, is represented in Fig. 20

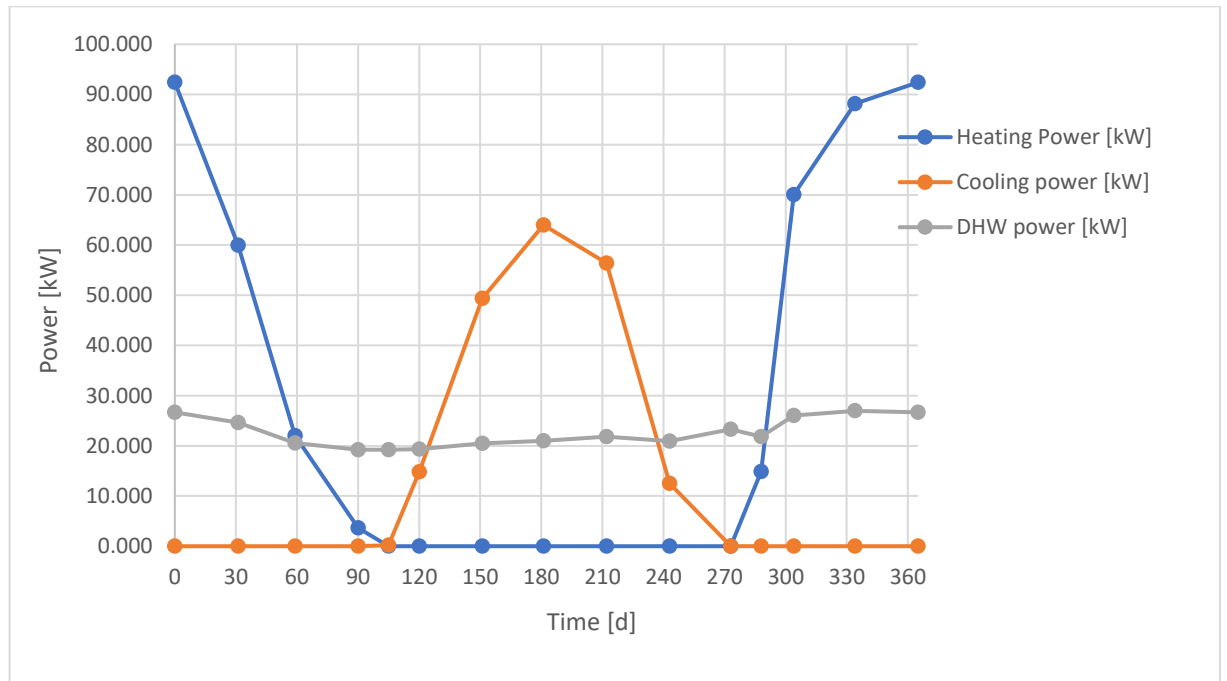


Fig. 20. Power demand in time.

The power of thermal plant is function of  $\Delta T$  parameter or rather the difference of temperature between extracted and injected groundwater, a value that must respect regional law; in Milan this limit is fixed to  $\pm 7$  K. In the case of study,  $\Delta T$  was assumed equal to  $\pm 5$  K.

In referment to Equation 1, is possible calculate respectively the extraction and injection constant flow according to the average power of thermal plant. The results are synthetised in Tab. 6, fixed  $c_p=1.16 \text{ kWh}\cdot\text{m}^{-3}\text{K}^{-1}$ .

Tab. 6. Extracted and injected flow rate.

| Time Interval [d] | Extracted flow rate [l/s] | Injected flow rate [l/s] |
|-------------------|---------------------------|--------------------------|
| 0                 | 2.852                     | - 1.901                  |
| 31                | 2.027                     | - 1.351                  |
| 59                | 1.020                     | - 0.680                  |
| 90                | 0.548                     | - 0.365                  |
| 105               | 0.456                     | - 0.304                  |
| 120               | 0.109                     | - 0.073                  |
| 151               | 0.692                     | - 0.461                  |
| 181               | 1.030                     | - 0.687                  |
| 212               | 0.828                     | - 0.552                  |
| 243               | 0.203                     | - 0.135                  |
| 273               | 0.557                     | - 0.371                  |
| 288               | 0.879                     | - 0.586                  |
| 304               | 2.140                     | - 1.427                  |
| 334               | 3.046                     | - 2.031                  |
| 365               | 2.852                     | - 1.901                  |

The value of extracted and injected flow rate shown in Tab.6, will be represented an input data to set the heat transport simulation, studies remanded to the next paragraphs.

### 2.3.2 The wells field

The project of GWHP provides 2 extraction wells and 3 re-injection wells, sited in a strategic way to exploit the hydraulic gradient, distant from each other 90 m. According to the WGS-84 coordinates system, the exactly position of each well is defined as follow:

- Extraction well 1: 45°30'45.03"N, 9°10'39.92"E.
- Extraction well 2: 45°30'44.84"N, 9°10'39.11"E.
- Re-injection well 1: 45°30'41.53"N, 9°10'38.00"E.
- Re-injection well 2: 45°30'41.94"N, 9°10'37.73"E.
- Re-injection well 3: 45°30'42.44"N, 9°10'37.35"E.

The position chosen for the wells represents the optimal arrangement (Fig. 21), specifically, the extraction well upstream and re-injection well down stream aligned with the groundwater flow.

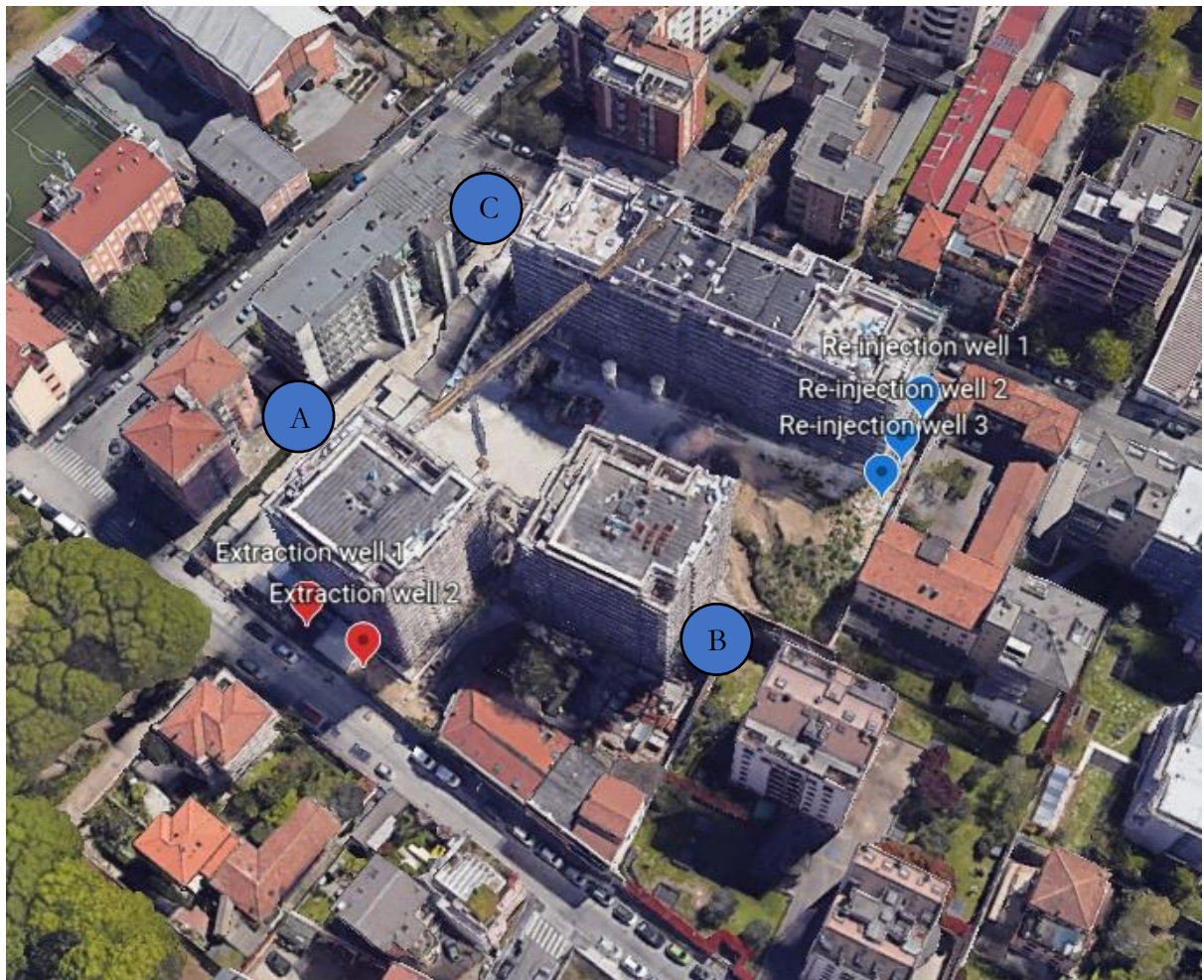


Fig. 21. 3D view of extraction and re-injection well position. Source: Google Earth.

During the drilling phases, for each well it was performed a max diameter equal to 0.08 m, reaching a depth of 40 m, condition which ensures an appropriate hydraulic head above the screen.

The 2 extraction wells are structured by PVC pipes of a diameter  $\varnothing_e$  equal to 400 mm and length 5 m, linked by a glass junction, reaching a depth of 40 m. The screened filter pipes, characterized by the same material and diameter of the previous one, are assembled in accord to the scheme shown in Fig. 22. The extraction wells are designed to extract an average flow rate equal to 12.2 l/s and a maximum flow of 29.6 l/s.

The PVC pipes are suitable for this kind of operations, able to guarantee high resistance to collapse and traction. Moreover, ensure high corrosion resistance, high durability and versatility to the grain size pack. [12]


| Profondità   | Stratigrafia   | Diametro e Schema di Filtraggio | Soggiacenza                              |
|--|--|---------------------------------|--|
| 0  |  | 400 mm                          |  |
|  | Ghiaia sabbiosa e ghiaia sabbioso limosa da umida a satura priva di evidenze di letti impermeabili di separazione. | 0                               |  |
|  |  | Cieco                           |  |
|  |  | -5                              |  |
|  |  | Cieco                           |  |
|  |  | -10                             |  |
|  |  | Cieco                           |  |
|  |  | -15                             |  |
|  |  | Cieco                           | - 17.80                                  |
|  |  | -20                             | ----                                     |
|  |  | Cieco                           | --                                       |
|  |  | -25                             |  |
|  |  | Cieco                           |  |
|  |  | -30                             |  |
|  |  | Filtro                          | Rilievi piezometrici a fine perforazione |
|  |  | -35                             |  |
|  |  | Filtro                          |  |
|  |  | -40                             |  |

Fig. 22. Scheme extraction well 1 and extraction well 2.

In the same way, the 3 re-injection wells are constituted by PVC pipes; in this case the diameter  $\varnothing_e$  is equal to 330 mm and, also in this case, the reached depth is 40 m. The assembly scheme is represented in Fig. 23. It is provided a screened filter pipes of diameter 330 mm. Each screened filter is characterized by a certain value  $R$  [l/s/m], defined like the ratio between the flow rate for unit of length of the screen, as follow:

$$R = \frac{Q}{L} = \pi D \cdot \alpha \cdot v_{ott} \quad \text{Eq. 7}$$

where:

- $D$  [m] is the diameter of the pipe.
- $\alpha$  [/] is a dimensionless parameter, which indicates the lateral surface of the pipe open to the flow of groundwater.
- $v_{ott}$  [m/s] is the optimal velocity of water at the screen, function of aquifer lithology, generally fixed equal to 0.03 m/s.

The extracted water, at the end of the cycle, will be injected in the subsoil by means the wells, generating a plume object of the next studies.


| Profondità   | Stratigrafia   | Diametro e Schema di Filtraggio | Soggiacenza                              |
|--|--|---------------------------------|--|
| 0  |  | 330 mm                          |  |
|  | Ghiaia sabbiosa e ghiaia sabbioso limosa da umida a satura priva di evidenze di letti impermeabili di separazione. | 0                               |  |
|  |  | Cieco                           |  |
|  |  | -5                              |  |
|  |  | Cieco                           |  |
|  |  | -10                             |  |
|  |  | Cieco                           |  |
|  |  | -15                             |  |
|  |  | Cieco                           | - 17.80                                  |
|  |  | -20                             | ----                                     |
|  |  | Cieco                           | --                                       |
|  |  | -25                             |  |
|  |  | Filtro                          |  |
|  |  | -30                             | Rilievi piezometrici a fine perforazione |
|  |  | Filtro                          |  |
|  |  | -35                             |  |
|  |  | Filtro                          |  |
|  |  | -40                             |  |

Fig. 23. Scheme re-injection wells 1,2,3.

## 2.4 Hydraulic characterisation of the aquifer

The aim of the hydraulic characterisation of an aquifer is to determine the hydraulic parameters through a series of tests. [13] These are transient pumping tests which are distinguished in:

- constant flow rate: measures the decrease of groundwater level keeping a constant pumping flow rate; moreover, can be performed also a step drawdown test;
- variable flow rate: performing sudden variation of level, measuring the recovery of undisturbed condition;
- rise level: at the end of a constant flow test, the rise level in the well is measured, till the complete recover of the undisturbed condition.

Furthermore, these kinds of tests are distinct in single or multi-wells, based on the number of observation and active piezometers necessary to make measurements.

#### 2.4.1 Step drawdown test

The step drawdown test consists of determining the relationship between the pumping flow rate and the losses head, linked to the drop of hydraulic level compared to the undisturbed condition of groundwater. Generally, it is performed imposing different values of pumping flow (not less than three values how shown in Fig. 24) until the undisturbed condition which is reached when the well doesn't undergo level variations after 30 minutes the start of test. [8]

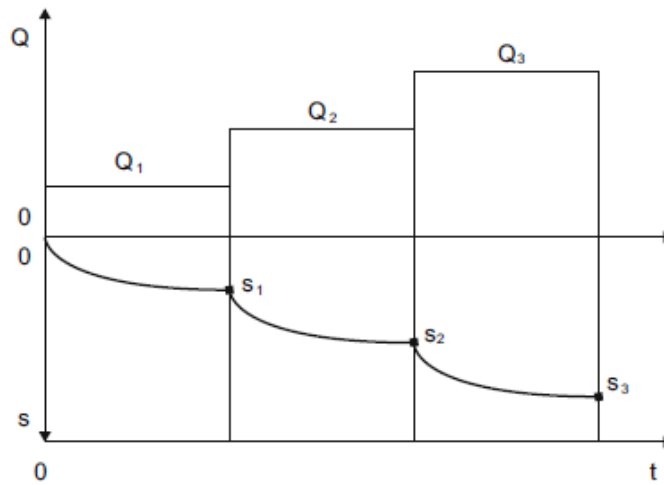


Fig. 24. Scheme related to step drawdown well test.

Theoretically, the interpretation of drawdown step tests is linked to Rorabaugh's equation:

$$s_m = (B_1 + B_2 + B_3)Q + CQ^n \quad \text{Eq. 8}$$

where:

- $s_m$ : stabilized hydraulic level [m].
- $(B_1 + B_2 + B_3)Q$ : total losses head, function of three contributes;  $B_1Q$  represents losses head due to groundwater flow,  $B_2Q$  is the losses head contribute linked to partial penetration of the well and finally  $B_3Q$  expresses the losses head due to the eventually presence of a permeability anomalies around the pumping area.
- $CQ^n$  ( $n \geq 2$ ) expresses the losses head concerning the presence of turbulent flow due to the flow through the filter.
- $Q$  is the pumping flow rate at which is performed the test.



In that case in which  $n=2$ , the equation is equal to:

$$s_m = (B_1 + B_2 + B_3)Q + CQ^2 \quad \text{Eq. 9}$$

more commonly called Jacob's equation. Experimentally, the objective is to determine the parameter of B, C and n that allow to define the  $s_m$ , so the drop of level due to a certain pumping flow rate. In this way is possible construct the characteristic curve of the well. An example of curve is shown in Fig. 25.

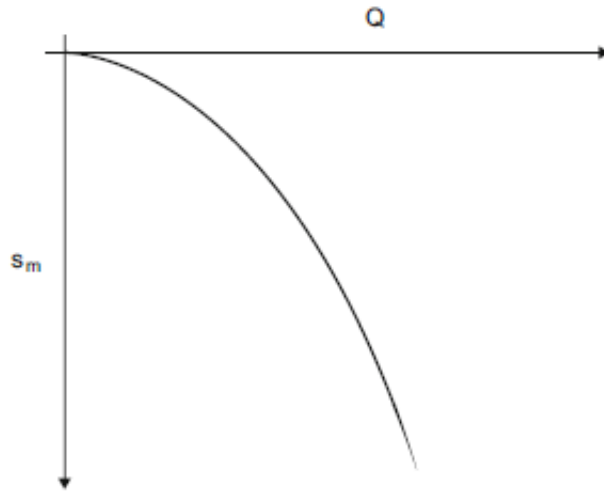


Fig. 25. Characteristic curve of a well.

In site, it is measured the undisturbed groundwater level through an electric level meter. Then, it is set a pumping flow rate of test using a flow meter, in line with the pumping system; at constant time intervals is measured the level of the groundwater until any variation of level is recorded.

In the developed case study, were conducted three pumping tests level, respectively for  $Q_1=4.39$  l/s,  $Q_2 = 9.89$  l/s,  $Q_3 = 14.51$  l/s, and the results are resumed in Tab. 7.

Tab. 7. Step drawdown test.

| Pumping rate<br>[l/s] | Static level<br>[m] | Drop level<br>[m] |
|-----------------------|---------------------|-------------------|
| $Q_1=4.39$            | 17.80               | 0.64              |
| $Q_2=9.89$            | 17.80               | 2.82              |
| $Q_3=14.51$           | 17.80               | 6.51              |

Then, the results of test are represented in a diagram, where in a y is fixed the drop of level s [m] and in x the corresponding flow rate Q l/s], getting a characteristic curve of the extraction well shown in Fig. 26.

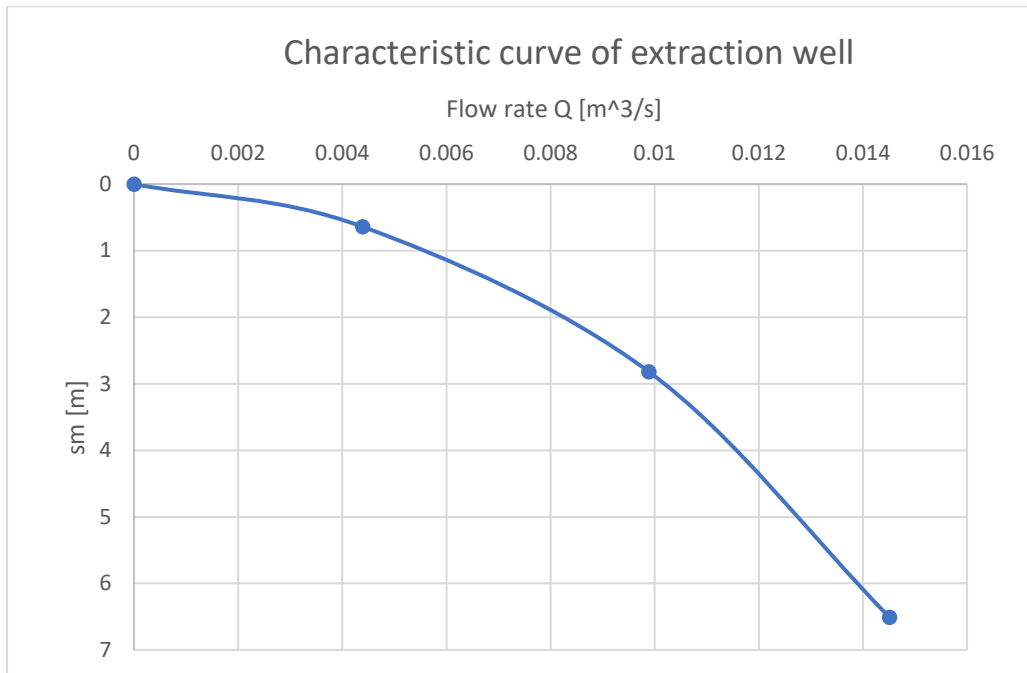


Fig. 26. Characteristic curve of extraction well.

#### 2.4.2 Long-term pumping test

The long-term pumping test is performed for a time varying between 48 and 72 hours at constant flow, determining the drop of level recorded in the extraction well, after pumping operations. Once reached the steady state condition, it is possible to evaluate the hydraulic conductivity by means of two piezometers distant respectively  $r_1$  and  $r_2$  to the extraction well, through which can determine the hydraulic head; especially, the value of conductivity is calculated thanks to the following equation, known as Dupuit - Thiem equation, useful for steady state conditions and unconfined aquifer:

$$K = \frac{Q}{\pi (h_1 + h_2) (\Delta h_{p1} - \Delta h_{p2})} \ln \frac{r_2}{r_1} \quad \text{Eq. 10}$$

whit:

- $h_1$  and  $h_2$  respectively the groundwater level detected in the two piezometers.
- $\Delta h_1$  and  $\Delta h_2$  hydraulic head compared to the undisturbed level of aquifer.
- $Q$  the pumping flow rate with which was performed the test is 12.2 l/s.

The observation piezometers were positioned respectively at distance  $r_1=0.30$  m and  $r_2=10$  m from the extraction well in which it was detected a hydraulic difference compared to undisturbed level of the aquifer equal to  $\Delta h_1=1.12$  m and  $\Delta h_2=0.03$  m. Taking into account the previous parameter values, the conductivity  $K$  results equal to  $1.43 \cdot 10^{-4}$  m/s. In Fig. 27 an operating scheme of long-term pumping test.





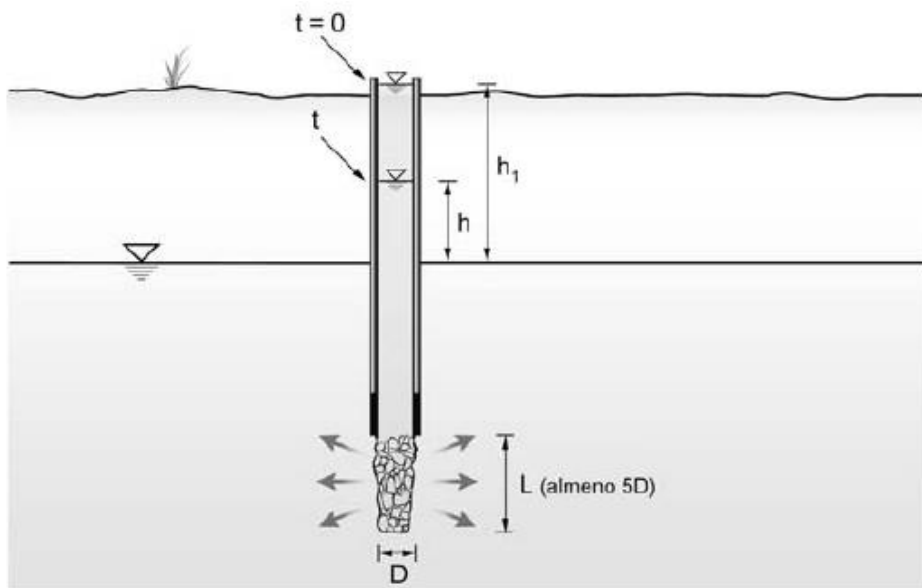


Fig. 28. Operation scheme of Lefranc test with constant head. Source: Ingegneria degli acquiferi [13].

Focusing the attention on the case study, it was conducted a Lefranc test, imposing a constant flow rate  $Q$  equal to 25 l/s. At the same time, the shape factor  $F$ , function of the two-dimension parameters of the well, equal to 32.17 m and  $\Delta h$  fixed to 2 m, average of all dynamic levels. The hydraulic conductivity  $K$  results equal to  $3.89 \cdot 10^{-4}$  m/s.

#### 2.4.4 ReInjection test

The reInjection test is executed to evaluate, consequently the injection of groundwater at the end of the plant cycle, the increasing of level in the well. Also in this case, is conducted a step test but regarded different injection flow rate, monitoring the raising with a water level device.

It was realized this test for each injection well, considering a different operating flow rate, according to the operating cycle of the thermal plant.

#### 2.4.5 Summary of the results

In conclusion, the tests shown some important results which represent an input data for the section 4, concerning the model of the geothermal plant.

All results regard the evaluation of hydraulic conductivity are resumed in Tab. 8.

Tab. 8. Experimental hydraulic conductivity.

| Hydraulic conductivity $K$ [m/s] |                        |
|----------------------------------|------------------------|
| Lefranc test                     | Long-term pumping test |
| $3.89 \cdot 10^{-4}$             | $1.43 \cdot 10^{-4}$   |

The 2 values of conductivity are the same order of magnitude and in some way this correspondence validates the result of tests. In the modelling phase will be adopted a  $K=3.89 \cdot 10^{-4}$ .

Furthermore, the step drawdown test evidence that the drop of level doesn't result excessive and does not undermine the operating of the plant.

Important underline how the previous evaluations are the result of standard test performed in site by specialized operators on which will base this study from hydrogeological point of view.

## 3 MONITORING SYSTEM

### 3.1 Groundwater monitoring

The groundwater monitoring system has the aim to detect a wide range of data regarded aquifer properties, for a long period, to study and manage the aquifer resource and its evolving in time. The main parameters monitored are groundwater level, temperature and quality of groundwater, exploiting a series of electronic devices called datalogger. These kinds of devices can measure and record data in a very accurate way, continuously at specific intervals of time.

#### 3.1.1 Monitoring network installed

The objective of the monitoring network installed in “Residenza Parco delle Favole” is to detect groundwater level and values of temperature; so, a representative series of data that allow to manage and predict the state of aquifer in the future.

In each well, (2 extraction wells and 3 re-injection wells) was installed a levelogger (Solinst Levelogger 5 model 3001), composed by stainless steel housing, resistant to corrosion and abrasion shown in Fig. 29. It is supplied of a pressure sensor (Fig. 30), offering high resolution and an accuracy of 0.05%, stable in extreme temperatures and pressure conditions, properties that make this device reliable for long term. The Levelogger 5 features a smooth, single-eye optical interface, which detect and record data at constant intervals of time. [15]. Each of them is supplied of a battery power system.



Fig. 29. Levelogger Solinst 5. Source: Solinst [15].



Fig. 30. Detail of single eye optical interface. Source: Solinst [15].

The installation procedures were preceded by a measurement of groundwater level for each well, using an electronic level meter sounder (Fig. 31). It is constituted by a sensor that at contact with the water table gives an acoustic signal. The next phase provides to manage the sensor in a way for which results completely standing on the free surface; a flat tape, permanently marked each millimeters, allows to evaluate the surface level depth, measured starting to the well border with an accuracy of 1-2 millimeters; moreover, were measured the bottom of each well with the same device.



Fig. 31. Water level meter sounder [16].

The results of preliminary surface water level measurements (evaluated starting to the top of well) are resumed in Tab. 9.

Tab. 9. Values of surface level of each well.

| Well name         | Water level [m] | Bottom of well [m] |
|-------------------|-----------------|--------------------|
| Extraction well 1 | 19.33           | 40                 |
| Extraction well 2 | 18.91           | 40                 |
| Injection well 1  | 17.99           | 40                 |
| Injection well 2  | 18.23           | 40                 |
| Injection well 3  | 18.12           | 40                 |

The levellogger must be set with a specific software, defining start time and period of data detection. It was imposed a recording step-time equal to 15 minutes. Once finish this operation it possible to proceed with the installation of datalogger in the well. It was predisposed an anchoring to the external surface of the well at which attach the datalogger by means a no extendable cable length around 25 m, thus allowing to be completely covered by column of water. The operation phases are shown in Fig. 32, Fig. 33, and Fig. 34.



Fig. 32. Levellogger setting.



Fig. 33. Anchorage levellogger to the external surface of the extraction well 1.



Fig. 34. Installation of levellogger.

The levelloggers collected data for 4 months, measuring and recording temperature and the absolute pressure. Important underline as the absolute pressure is determined like the sum of the water column above the levellogger pressure sensor  $P$  and the atmospheric pressure  $P_{atm}$ , acting on the water surface. For this reason, it was installed a barologger which records at constant intervals of time the atmospheric pressure. The device must be allocated in such a way to avoid any kind of interferences. It was installed in a space protect from distortions and vandalism, like shown in Fig. 35 and Fig. 36.



Fig. 35. Barologger placing.





Fig. 36. Detail barologger placing.

### 3.1.2 Analysis of monitoring data

The results of monitoring system are shown in Fig. 37. The monitoring began on 8 July 2022 and ended on 25 November 2022. In this period, it was recorded an increasing of groundwater level in each well. This trend may be the result of rainy events, which are more frequent during autumn and winter than summer; a phenomenon that recharge the natural resource. This aspect doesn't affect the performance of geothermal plant.

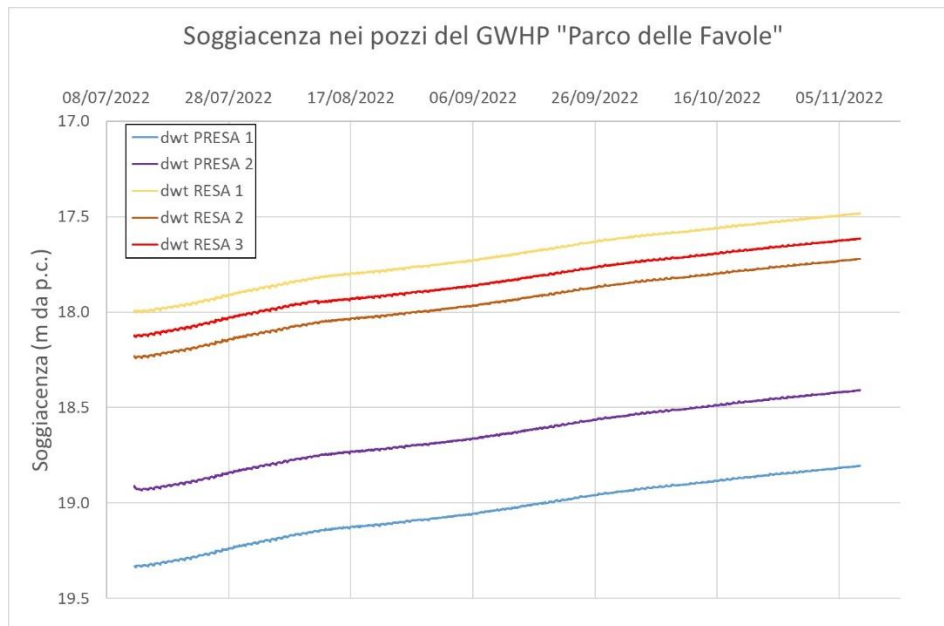


Fig. 37. Analysis of monitoring data.



### 3.2 Flow rate monitoring system

The monitoring of flow rate is a tool with the aim to manage the adduction system and check the correct operating of extraction pump. These kinds of monitoring are performed in different way, exploited a wide range of devices. The attention is focused on the ultrasonic flow meters, device installed in this case study.

The ultrasonic flow meter operating principle bases on acquisition of traveling time differences of a ultrasonic signal through a fluid. This system exploits two transducers that function as both ultrasonic transmitters and receivers, clamped at a specific distance from each other on the external surface of the pipe. The operating scheme is shown in Fig. 38.



Fig. 38. Ultrasonic flow meter.

The installation methods of transducers are function of the diameter of pipe and liquid characteristics, with the aim to maximize and perform the accuracy of measurements. As follow, are described three installation methods:

- V method: the sound transverses the pipe twice, so the path shape of signal is a V, for daily measurement with pipe inner diameters ranging from 15 mm to 200 mm [17] (Fig. 39).
- W method: the sound transverses the pipe four times, following a W path shape, usually used on pipes with a diameter from 15mm to 50mm [17] (Fig. 40).
- Z method: the sound crosses the pipe once because the transducers are mounted on opposite side of the pipe, used when the pipe diameter is above 200 mm [17] (Fig. 41).

The flowmeter operates by alternately transmitting and receiving a frequency modulated burst of sound energy between the two transducers and measuring the transit time that it takes for sound to travel between the two transducers.

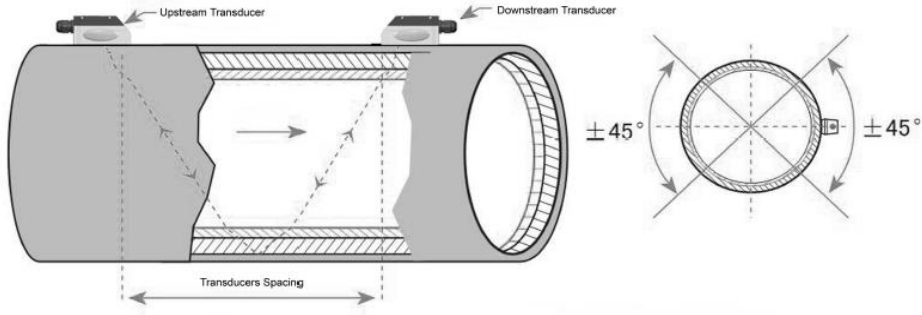


Fig. 39. V method installation [17].

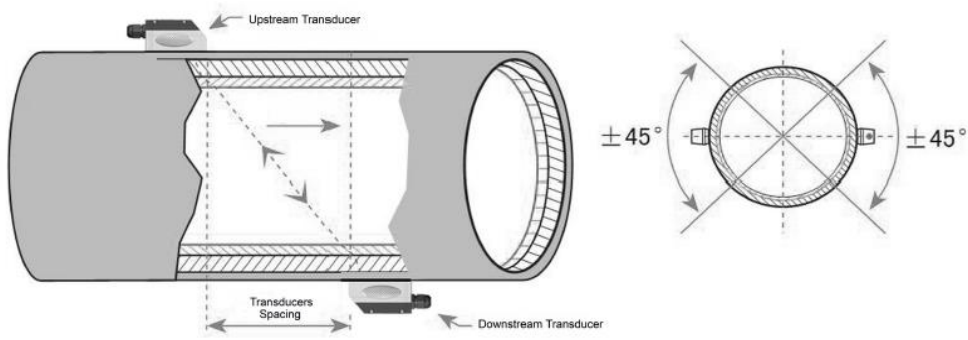


Fig. 40. Z method installation [17].

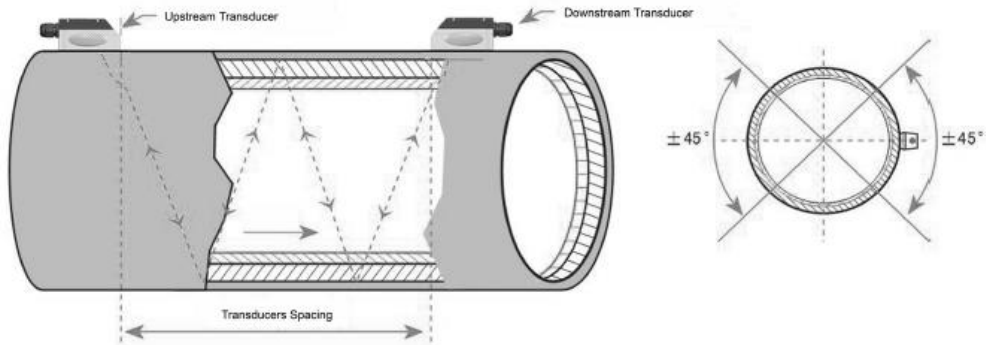


Fig. 41. W method installation [17].

The difference in the transit time measured is directly related to the velocity of the liquid in the pipe [17], following the equation:

$$V = \frac{MD}{\sin 2\theta} \cdot \frac{\Delta T}{T_{up} \cdot T_{dw}} \quad \text{Eq. 12}$$

where:

- $\theta$  is the include angle to the flow direction.

- $M$  is the travel times of the ultrasonic beam.
- $D$  is the pipe diameter.
- $T_{up}$  is the time for the beam from upstream transducer to the downstream one.
- $T_{dw}$  is the time for the beam from downstream transducer to the upstream one.
- $\Delta T$  is equal to  $T_{up} - T_{dw}$ .

Some expedients must be considered during installation phases:

- install the devices on the straight pipe with a sufficient length, constant diameter and completely full of liquid;
- to obtain better results is recommended clean the surface of the pipe before the installation of the transducers to eliminate any dust and rust;
- apply adequate coupler to the spot where the transducers are to be installed and leave no gap between the pipe surface and the transducers;
- to avoid gas bubbles inside the upper part of the pipe, the transducers should be installed horizontally by the side of the pipe;
- eliminate every kind of interferences that complicates the right procedures of measurement and installation.

## 4 SUBSURFACE FLOW AND HEAT TRANSPORT MODELLING

The section 4 is reserved for the analysis of subsurface flow and heat transport, building a numerical model that simulates the real operation of the open-loop geothermal system, exploiting a software called FEFLOW 7.5 (Finite Element subsurface FLOW and transport system). It's an interactive groundwater modelling system used, for example, to model geothermal processes, to estimate the duration and travel times of chemical species in aquifers, to plan and design remediation strategies and interception techniques, and to assist in designing alternatives and effective monitoring schemes.

It will be defined the domain of interest, paying attention to the other geothermal plants distributed on the territory which can affect the groundwater and thermal plume. Moreover, will be set boundary conditions, parameters of aquifer and operating cycle of the plant in order to simulate the transport of thermal plume, results on which will be conducted studies and considerations concerning the natural alteration of groundwater and future previsions.

### 4.1 Flow and heat transport in porous media

The heat transfer mechanism based on the principle of thermodynamic that defines the ways in which is transferred energy between bodies.

The heat transfer mechanism can be resumed as follow:

- conduction: heat transport occurs from zones at higher temperature to zones at lower temperature, due to the transmission of the agitation of molecules;
- advection: heat transport by a fluid due its overall motion;
- dispersion: heat transport due to the heterogeneity of the flow field.

Especially, the conduction, from mathematical point of view, is described by the Fourier law, defined as follow:

$$j_{c,xi} = -\lambda \frac{\partial T}{\partial x_i} \quad \text{Eq. 13}$$

where:

- $J_{c,x1}$  [W/m<sup>2</sup>] is the conductive heat flux in the  $x_1$  direction.
- $\lambda$  [W/mK] is the thermal conductivity.
- $\partial T / \partial x_i$  is the thermal gradient in direction  $x$ .

The minus (-) in the Eq. 13 considers that the flux of heat for conduction moves from higher temperature to lower temperature.

The advective flux  $J_{c,x1}$  is proportional to the Darcy velocity  $v_d$  according the follow equation:

$$j_{c,xi} = -v_d \rho_w c_w T = v_e n_e \rho_w c_w T \quad \text{Eq. 14}$$

whit:

- $v_e$  [m/s] effective velocity.
- $n_e$  [/] effective porosity.
- $\rho_w$  [kg/m<sup>3</sup>] density of water.
- $c_w$  [J/KgK] specific heat.
- $T$  [K] temperature of fluid.

While, the dispersion mechanism, occurs in porous media for the heterogeneous characteristics of the medium ( $v_e > 0$ ). The thermic dispersion is defined as follow:

$$j_{Dc,xi} = -\rho_w c_w \alpha_{xi} v_e \frac{\partial T}{\partial x_i} \quad \text{Eq. 15}$$

In this case appears the thermal dispersivity  $\alpha_{xi}$  [m], a parameter function of the referment scale, responsible of the spread of plume through time along and perpendicular to the flow direction. For this reason, it is distinguished in  $\alpha_L$  and  $\alpha_T$ , respectively longitudinal and transverse dispersivity.

At the same time, comparing to the transport of solute in a porous media, heat is subjected to sorption. The concept of sorption of heat is linked to the condition of temperature equilibrium between fluids which passes through a solid phase, leading to a delay in the rate of heat flow. In fact, the velocity of heat propagation is function of a retardation coefficient  $R_{th}$  defined as follow:

$$R_{th} = 1 + \frac{1 - n_e \rho_s c_s}{n_e \rho_w c_w} \quad \text{Eq. 16}$$

whit

- $\rho_s c_s$  [kg/m<sup>3</sup>] the thermal capacity of the solid.

It follows that the velocity of heat propagation  $V_{th}$  result equal to:

$$V_{th} = \frac{V_e}{R_{th}} \quad \text{Eq. 17}$$

So, the velocity of thermal flux will result lower than the effective velocity for effect of sorption.

In conclusion, the general equation that describes the heat transport and considers all mechanisms analysed until now is defined as follow:

$$\frac{\partial T}{\partial t} + D_x \frac{\partial^2 T}{\partial x^2} + D_y \frac{\partial^2 T}{\partial y^2} + D_z \frac{\partial^2 T}{\partial z^2} - v_{th} \frac{\partial T}{\partial x} = \frac{H}{\rho c} \quad \text{Eq. 18}$$

where:

- $H$  [W/m<sup>3</sup>] is the thermal source or sink.

- $D_x$  [ $m^2/s$ ] is the dispersion coefficient along the groundwater flow direction.
- $D_y$ ,  $D_z$  [ $m^2/s$ ] are the thermal dispersion coefficient transversally to groundwater flow, respectively in direction  $y$  and  $z$ .

In the next paragraphs the different phases of model design, step by step, supplying all graphic and numerical results.

## **4.2 Development of the numerical model**

### **4.2.1 Conceptual model**

The conceptual model is a descriptive representation of groundwater system that incorporates the interpretation of the geological and hydrogeological conditions. The aim of the model is to simulate the operating cycle of geothermal plant, paying attention to the evolution of thermal plume and the effects on the natural system.

Conceptually, a model is a means to represent reality in a simplified way. The objective is to build a model system characterised by complexity level proportional to the expected result; higher is the numbers of information, higher will be the complexity of model.

The first assumption on which based the model regards the hydrogeological compart; as defined in section 2, the area of Milan is characterized by the presence of two main hydrogeological formations, distinct by nature and grain size composition. The shallow aquifer, which extends till a depth of 100 m, more permeable compared to the deeper layers characterized by silty formation. For this reason, the hydrogeological field of analysis will be modelled considering the shallow aquifer limited at the bottom by a low permeable horizon; this allows to manage a simplified domain, limited ad the bottom, representative of the real state of site.

### **4.2.2 The modelling domain**

The domain of interest is shown in Fig. 42: a rectangular area (3079.50 m x 3348 m) extended from north to south respect to the reference system that incorporates the building site and the open-loop plant. The area intercepts also other geothermal plants and piezometers distributed on the territory of Milan with the aim to exploit them as monitoring point for the following analysis. To simplify the study, the domain is limited between two iso-piezometric curves, corresponding to the groundwater level, respectively 120 m 110 m; while the 5 wells are identified by 5 points as shown in Fig. 43.

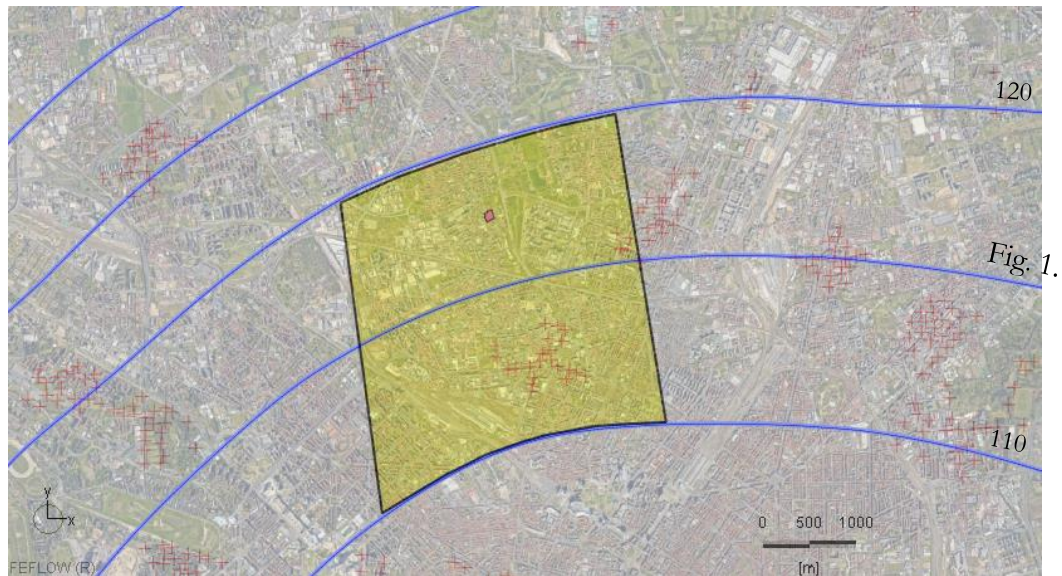


Fig. 42. Model domain.



Fig. 43. Detail area of interest and wells.

In FEFLOW, a preliminary step regards the generation of Finite-element Mesh (FeM), a set of limited geometrical elements number, defined by lines and nodes, generating a 2D mesh.

On it will based the building of model in terms of plant components, properties of aquifer, boundary conditions etc. The software FEFLOW presents different options to design a mesh based on the choice of elements shape. For the purposes of this study, it was adopted a triangular meshing how shown in Fig. 44. Important underline how the density of the mesh is proportional to the better numerical accuracy and higher computational effort; for this reason, in a specific or relevant points object is good role increasing the number and the regularity of the elements because many distortions can arise during the simulation if the mesh is much irregular.



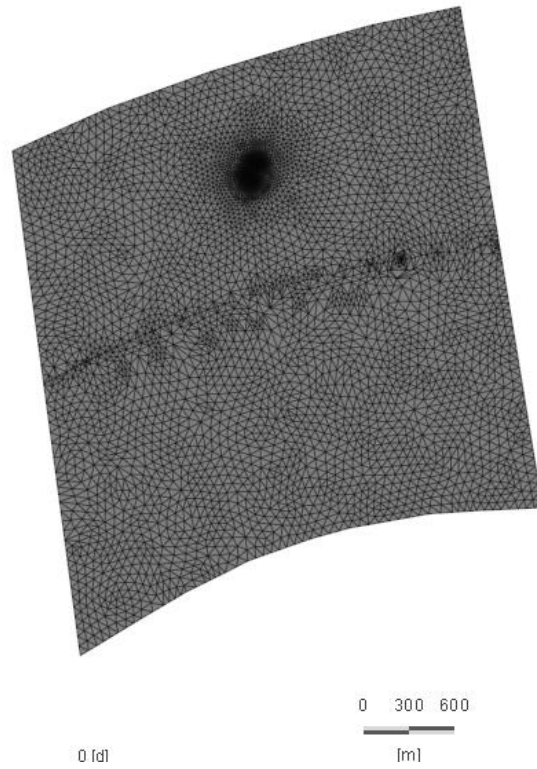


Fig. 44. Meshing domain.

To refine the mesh, it was used the option 2D mesh smoothing, to confer more regularity and symmetry for triangles, solution represented by a mesh mostly composed of equilateral triangles. More importance is reserved for the wells where, how anticipated before, needs to pay particularly attention to be sure that result is as real as possible. A spatial discretization imposes the exactly position of nodes around each well; it was chosen a hexagonal distribution shown in Fig. 45.

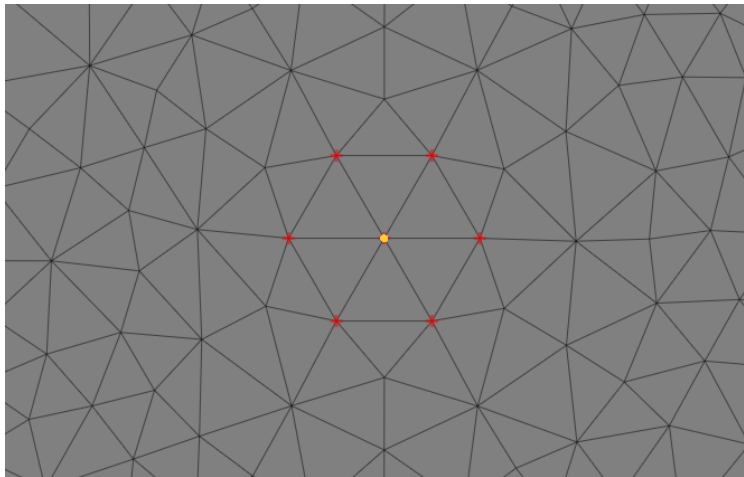


Fig. 45. Discretization of wells points.

The next step regards the spatial resolution of domain (3D). Taking into account all hydrogeological information of the site, it was fixed a thickness of the domain equal to 100 m corresponding to the overage depth of shallow aquifer in that area. Then, split in layers and slices, whit the aim to model the real geological state of the subsoil. In particular, was fixed 8 layers defined by 9 slices. Once

imposed the upper slice fixed at 135 m asl and the deeper at 35 m asl, the software automatically calculates the distribution of all slices, values resumed in Tab. 10. The slices distribution has the aim to models the subsoil stratigraphy, useful to assign at each of them different properties concerning aquifer and geothermal plant. The slice 1 correspond to the earth's surface and slice 9 the fixed no permeable limit. Then, the slices 2, 3 and 4 correspond to the active part of the geothermal plant, corresponding to the water table of the groundwater and the screen filter of the wells. Deeper to the slice 4 corresponds to the bottom of the well, which was discretised in slice 5,6,7 to evaluate result in more gradually way at different depth. The 3D view is shown in Fig. 46.

Tab. 10. Slice overage altitude.

| Slice   | Altitude<br>[m asl] |
|---------|---------------------|
| Slice 1 | 130.711             |
| Slice 2 | 112.711             |
| Slice 3 | 100.711             |
| Slice 4 | 90.711              |
| Slice 5 | 79.711              |
| Slice 6 | 68.711              |
| Slice 7 | 57.711              |
| Slice 8 | 46.711              |
| Slice 9 | 35.711              |

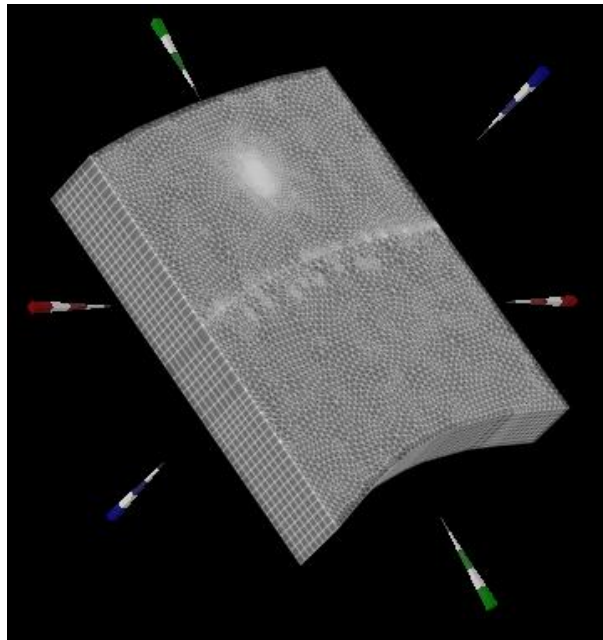


Fig. 46. Model 3D view.

In conclusion, the model is based on 110'960 element and 63'450 nodes that compose the 3D mesh.

### 4.2.3 Modelling setup

Once defined the geometry of the model it necessary to assign initial and boundary conditions, so that it can represent the real state of site. It's fundamental assigned the elevation for the north and south side of domain, corresponding to the real altitude value found from DEM (Digital Elevation Model) of Lombardia. The defined mesh allows to set a series of nodes at which assign a specific altitude value just selecting that nodes overlap with the boundary. Higher is the number of nodes, better will be the final linear interpolation to avoid dispersion of information and a more accurate interpretation of elevation level of the earth surface. Specifically, it was fixed an elevation value equal to 138 m for north limit and 125 m for south limit. Giving the elevation inputs, the software automatically, by means a linear interpolation, calculates for each node of the net the elevation value. The result is shown in Fig. 47.

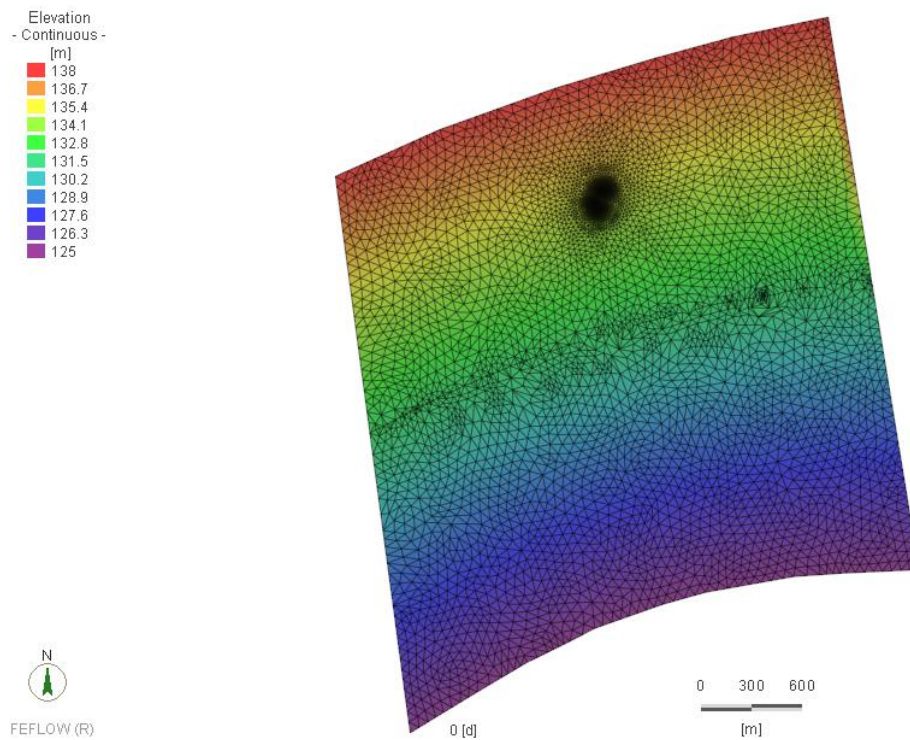


Fig. 47. Elevation model.

Similarly, boundary conditions were set respectively 120 m for the norther side and 110 for the southern side, according to the piezometric distribution.

Until now have been defined a part of the input parameters and structures useful to define an operating model; in the same way will identify each well, specifying depth, dimensions, and flow rate.

For each well, according to the design of the geothermal plant, it was fixed a radius equal to 0.40 m and a screen filter thickness, that extends till a depth of 40 m (slice 4), equal to 10 m.

The setting of flow rate is based on time series inputs, by means was defined the couple of values (Time [d], Pump rate [l/s]) to indicates the operating cycle of the system, applied to the model

cyclically, each of them individuated by a specific ID. The result of settings is shown in Fig. 48 and Fig. 49, respectively for an extraction well and injection well. The couple of data Time - Pump Rate is a result developed in section 2, concerning the operating power of the plant. For convention it was adopted minus for re-injected groundwater. The software will recognize for each well the corresponding time series rate, defining the operating cycle of plant.

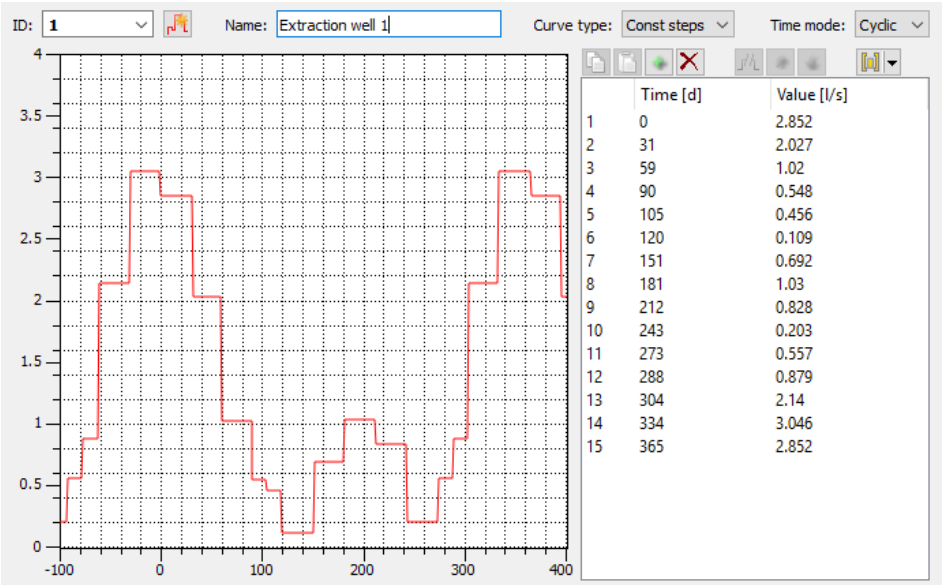


Fig. 48. Times series extraction well 1, 2.

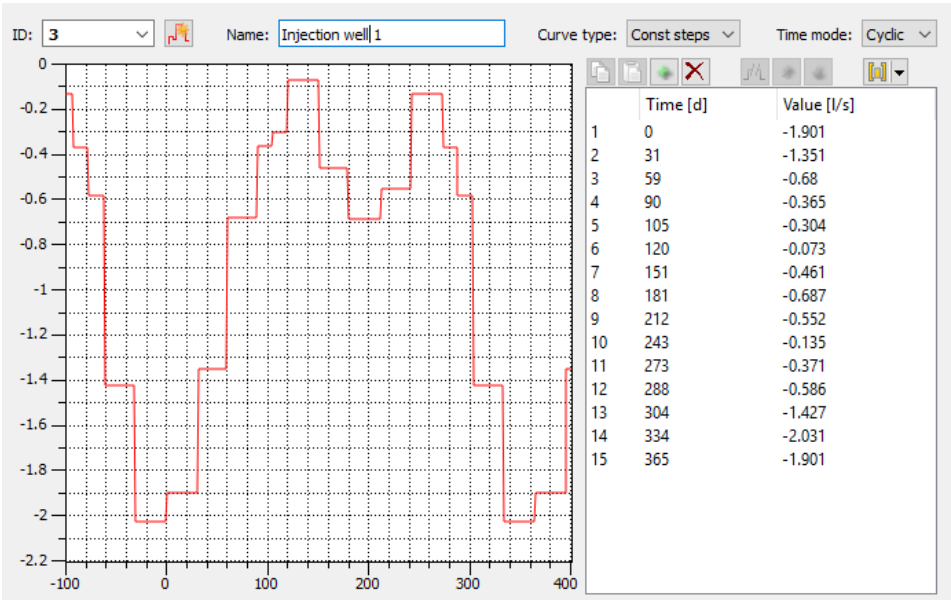


Fig. 49. Time series injection well 1, 2, 3.

Other important step regard setting of boundary conditions of the aquifer. Specifically, hydraulic boundary conditions define the water level surface of aquifer from north to south of the domain. How anticipated before, it was fixed hydraulic head equal to 120 m and 110 m respectively for north border

and south border, while by means a linear interpolation FEFLOW calculates the overage hydraulic head distributed on total domain obtaining a result in Fig. 50.

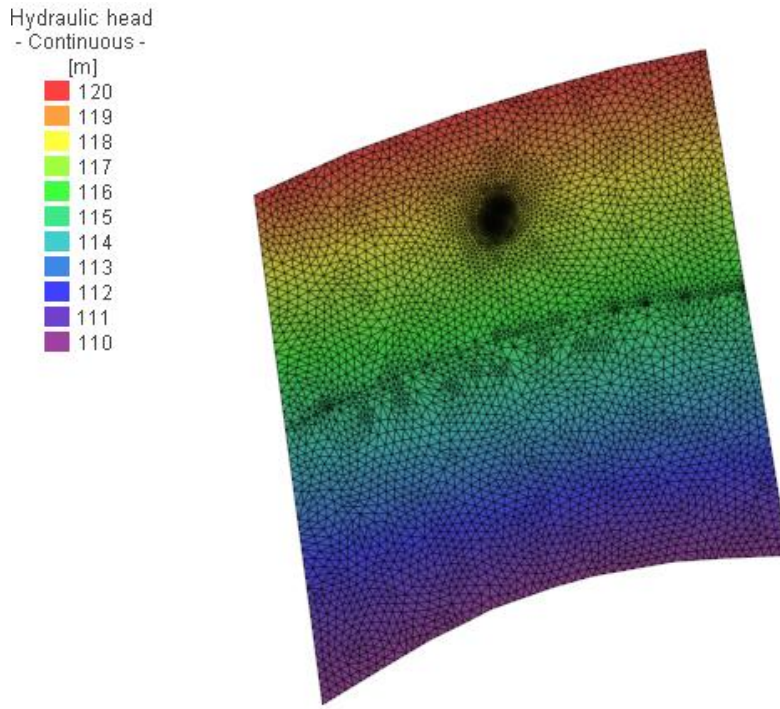


Fig. 50. Hydraulic head distribution.

It was fixed the hydraulic conductivity of the shallow aquifer, considering the anisotropy of hydrogeological formation. From literature, this condition is characterized by different value of hydraulic conductivity in referment to direction of flow, condition that is translate in  $K_{xx} \neq K_{yy} \neq K_{zz}$ , once fixed an opportune coordinate system.

In this case it was assumed:

$$K_{xx} = K_{yy} = 0.1 \cdot K_{zz} \quad \text{Eq. 19}$$

In reference to the section 3,  $K_{xx}$  is assumed equal to  $3.89 \cdot 10^{-4} \text{ m/s}$  and from equation 19,  $K_{zz}$  results equal to  $3.89 \cdot 10^{-5} \text{ m/s}$ . These values were extended to all slices, except for slice 9, the deeper one, where in reference to the previous dissertation was imposed less permeable that the shallower ones, at which corresponds  $K_{xx} = 1 \cdot 10^{-8} \text{ m/s}$  and  $K_{zz} = 1 \cdot 10^{-9} \text{ m/s}$ , typical hydraulic conductivity values of clayey geological formation. The 3D view evidences this characterization, shown in Fig. 51 and Fig. 52.



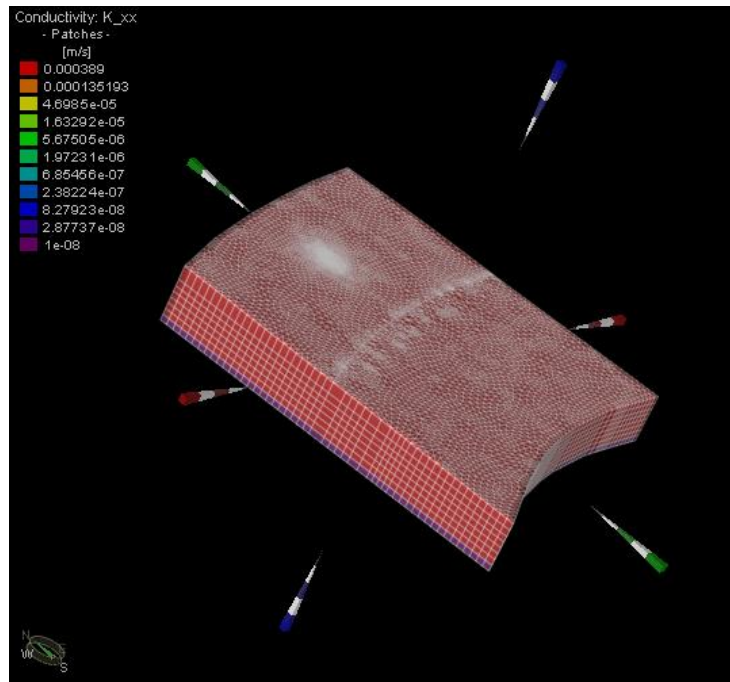


Fig. 51. 3D view hydraulic conductivity distribution ( $K_{xx}=K_{yy}$ ).

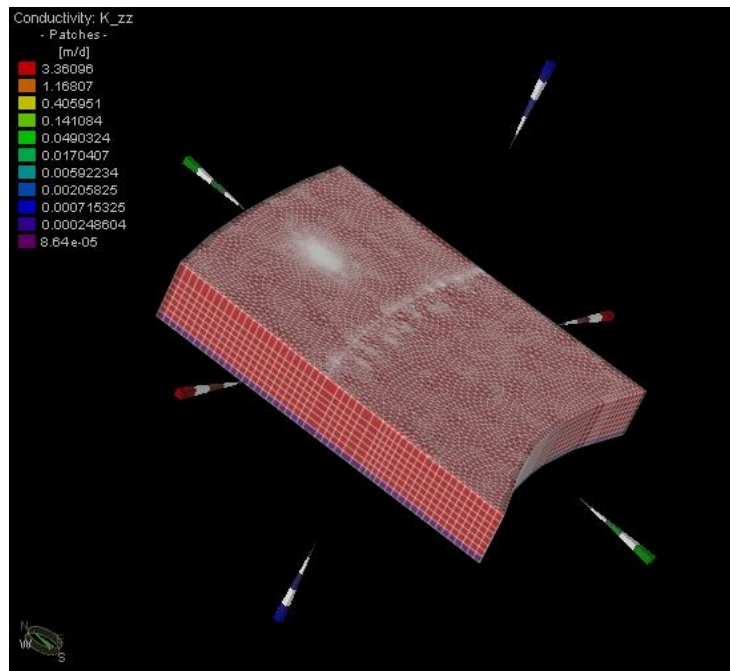


Fig. 52. 3D view hydraulic conductivity distribution ( $K_{zz}$ ).

The heat transport simulation requested to impose the temperature conditions, corresponding to the overage temperature of groundwater in an undisturbed state. The temperature was set equal to 15°C on the base of monitoring result installed in site. Furthermore, the porosity of the hydrogeological formation is fixed at 0.2.

Subsequently, once determined the aquifer parameters, it possible set the open-loop system; the software recognize the path between extraction and injections wells, simply assigning a specific value

for each well-node distinct from other nodes that composes the mesh. In this way, during simulation, it will be defined a flow path starting to extraction wells to be injected in the 3 wells downstream, originating a thermal plume functions of boundary conditions of domain. The well's view is shown in Fig. 53.

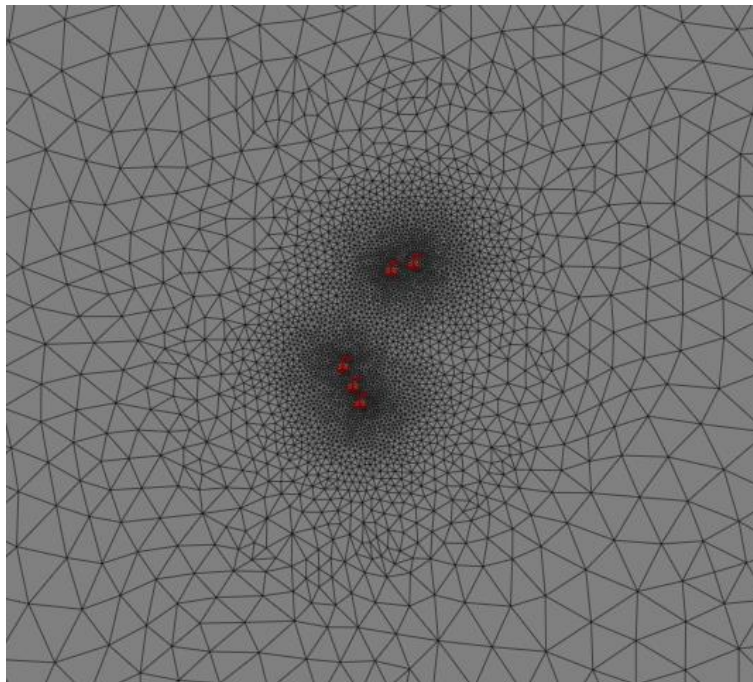


Fig. 53. Open-loop plant system setting.

In Fig. 54. the thermal jump, result of section 2 analysis, to set the operating cycle of open-loop plant.

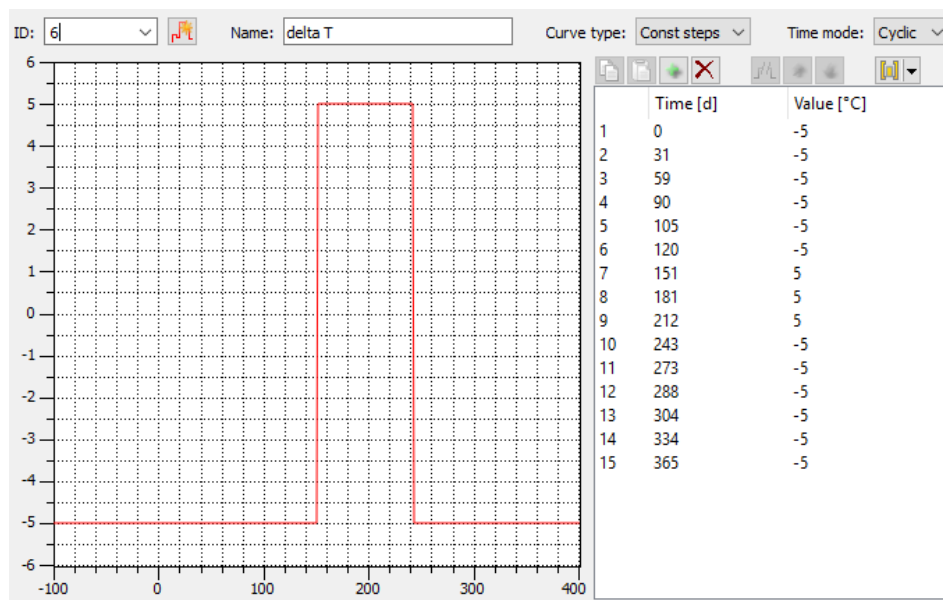


Fig. 54. Thermal jump open-loop plant

The heat transport simulation is preceded by the positioning of the representative observation wells in order to monitor the results and trend thermal plume evolved in time. Their position is shown in



Fig. 55. The simulation time was fixed for a representative time of referment equal to 3650 days (10 years); moreover, the evolution of thermal plume in time was evaluated in transient conditions.

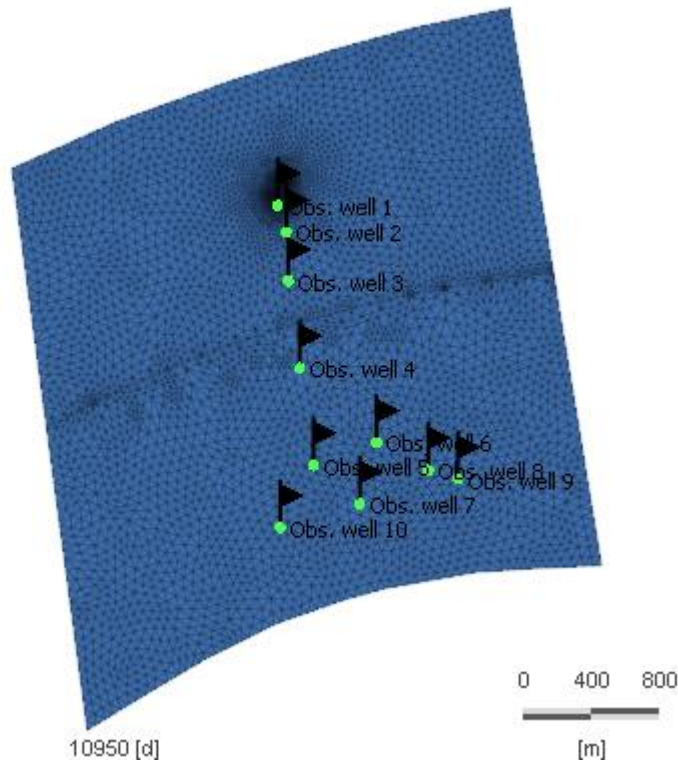


Fig. 55. Observation wells.

The analysis regarded the impact of thermal plume in time is explained in the next paragraphs, discussing different operating mode impact, future scenarios and available manage solutions.

### 4.3 Results and discussion

The simulations of heat transport put in evidence the thermal impact of geothermal plant compared to the undisturbed state of aquifer. The next figures have the aim to show the development of thermal plume, especially in different period of the year, conditions that explain the different operating cycle of the plant, respectively heating and cooling mode.

In Fig. 56 is shown the thermal plume after 3504 days the starting operating date of geothermal system, coinciding with the month of July (cooling mode), instead in Fig. 57 the thermal plume after 3650 days, corresponding to month of December (heating mode). First important result is that in both case the thermal plume doesn't involve any other geothermal plants installed on the area of Milan (yellow points). This is due to the low entities of the geothermal plant and injected flow rate from an operating point of view.



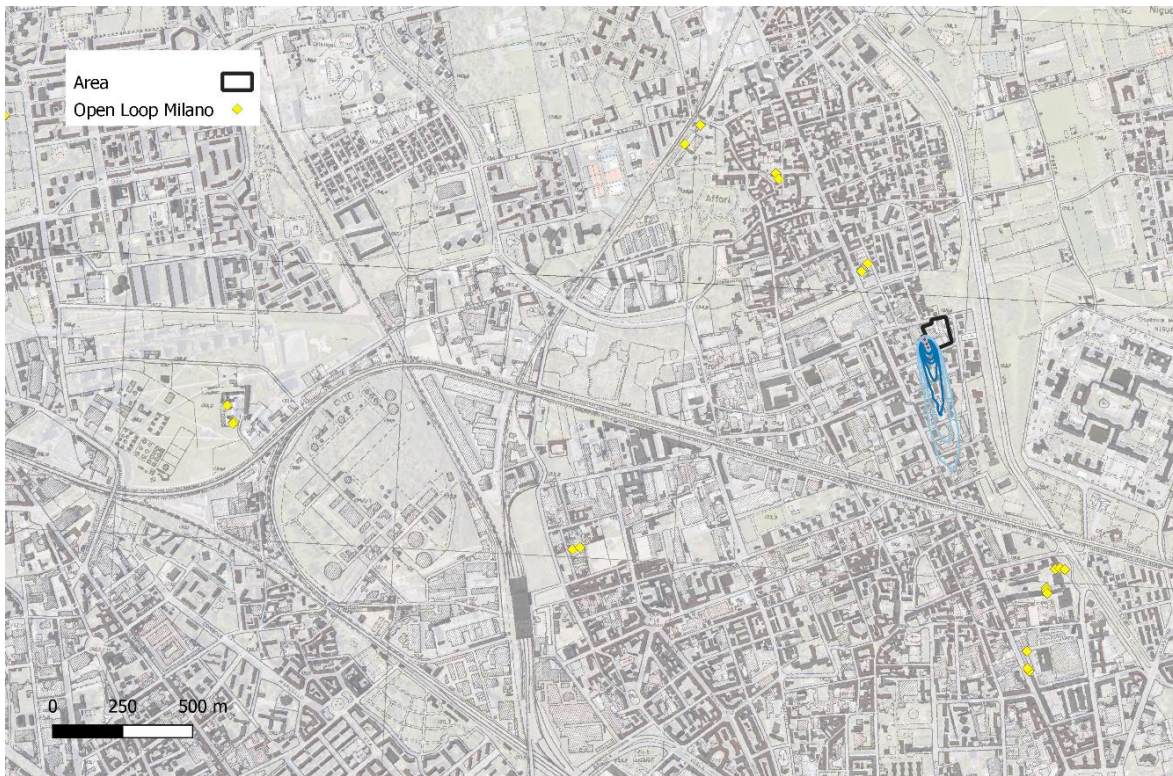


Fig. 56. Thermal plume after 3504 days (cooling mode).

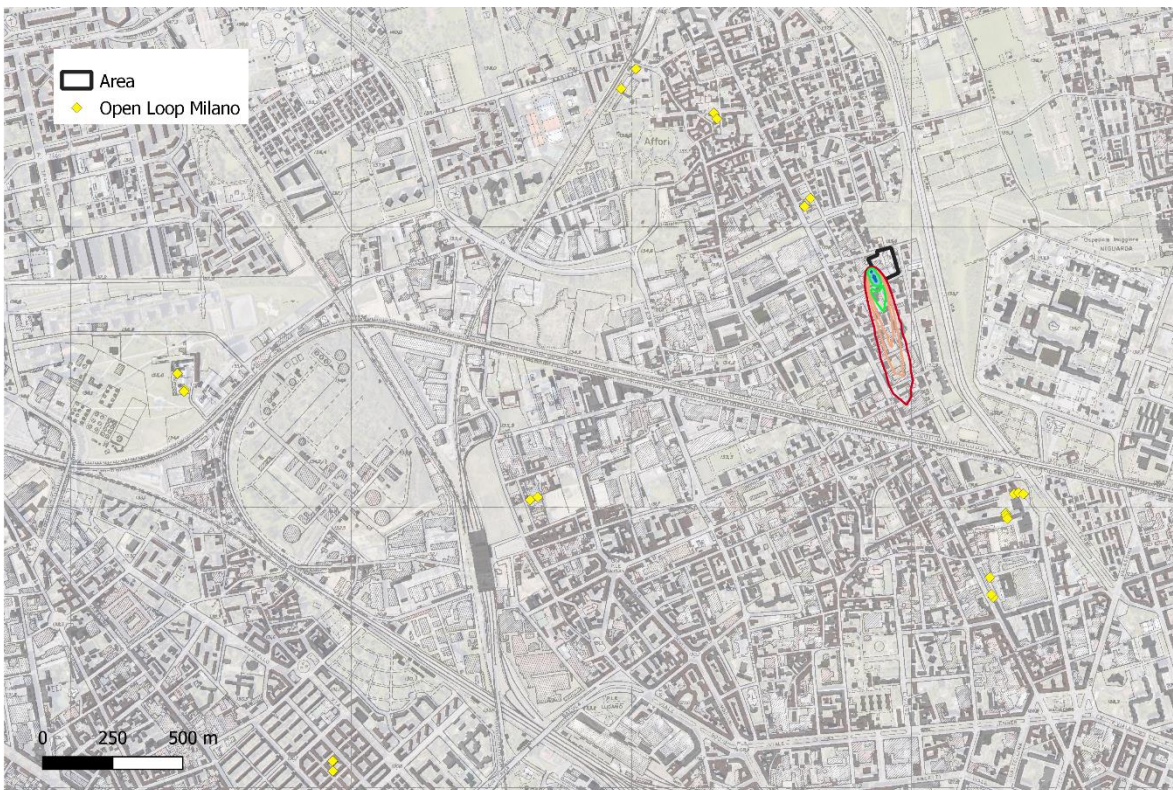


Fig. 57. Thermal plume after 3650 days (heating mode).

In Fig. 58 and Fig. 59 a detail of two thermal plumes that evidence the absence of thermal recycling, ensuring the optimal performance and design of plant.





Fig. 58. Detail of thermal plume after 3504 days (cooling mode).

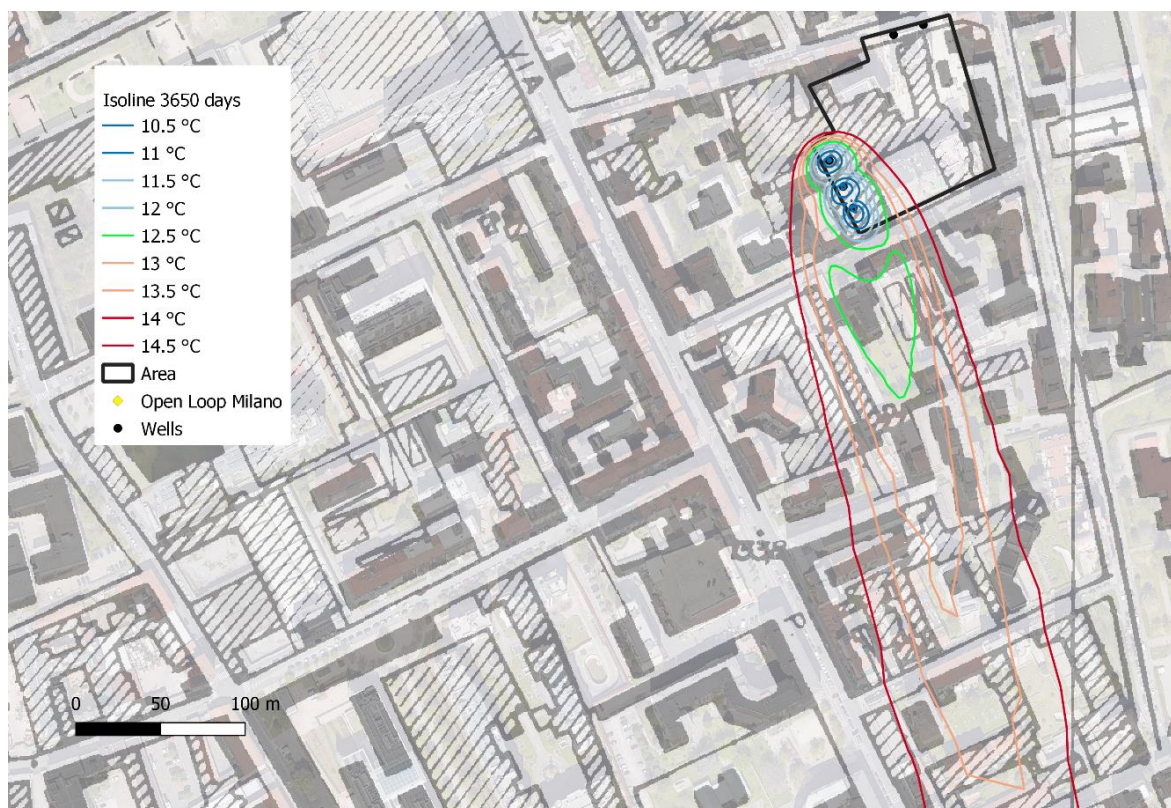


Fig. 59. Detail of thermal plume after 3650 days (heating mode).

Moreover, it notes that around the injection well during the summer is injected a hot water (peak of 18.5 °C), instead during winter cold water (peak of 10.5°C). This is a result of heat exchange mechanisms performed by heat pumps during the two operating mode. The temperatures detected around the injection wells are gradually attenuated till the undisturbed temperature state, condition due to dispersion phenomena. As shown in Fig. 59 the total area occupied by thermal plume, considering the 14 °C isoline, closer to the temperature of equilibrium,

In Fig. 60 the longitudinal section of the thermal plume corresponding to 1504 operating days. It shows how the plume involves most the shallower layers, finding a limitation in the deeper ones, where the temperature remains stationary. The hot fluid is dispersed and diluted achieving the equilibrium downstream the emission.

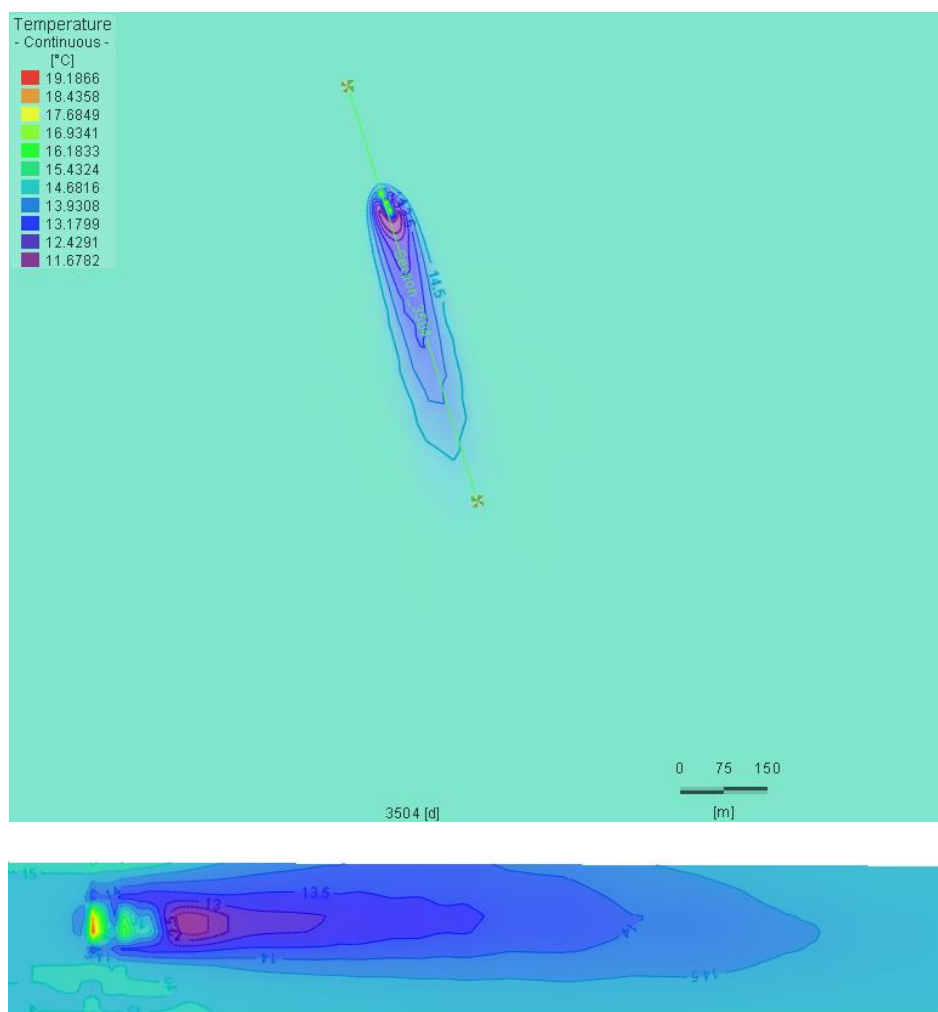


Fig. 60. Longitudinal section of thermal plume (3504 days).

In Fig. 61 the longitudinal section of thermal plume corresponding to 3650 operating days. The result obtained in this case are exactly the same of the previous one, but opposite.

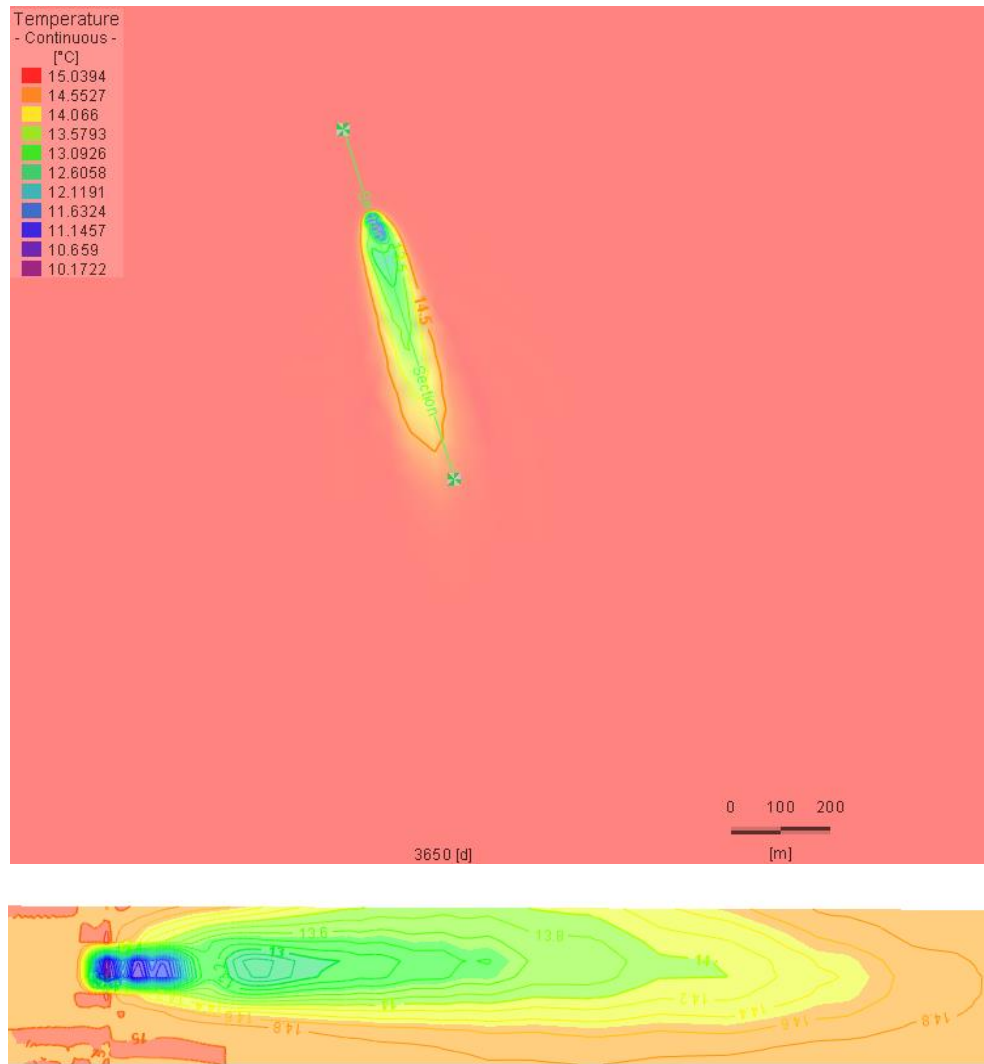


Fig. 61. Longitudinal section of thermal plume (3650 days).

In both cases the maximum extension of plume, considering a minimum variation of ground temperature of 1 °C is around 500 m, involving each layer of analysis. The low impact of thermal plume could be exploited to conduct a study regards the sustainable density of installed of shallow geothermal plant. The aim is to evaluate the print of plume corresponding to the 14 °C isoline, respectively for 3504 and 3650 days. This isoline is representative because proximate to the undisturbed temperature of groundwater, limit of thermal impact. However, the higher gradients of temperature are recorded around the wells. After 10 years, as shown in Fig. 62, approximately the two isolines concur, reaching the steady state condition. In referment of this analysis, could be studied in preliminary way the sustainability density of shallow geothermal plant installed on a certain area. As shown in Fig. 63, approximately the two isolines concur, for which is possible define a rectangular area equal to  $56 \cdot 100 \text{ m}^2$ , (110 m x 510 m) within is supposed happen the representative variations of temperature. to account the area of influence generated by this kind of shallow geothermal system.



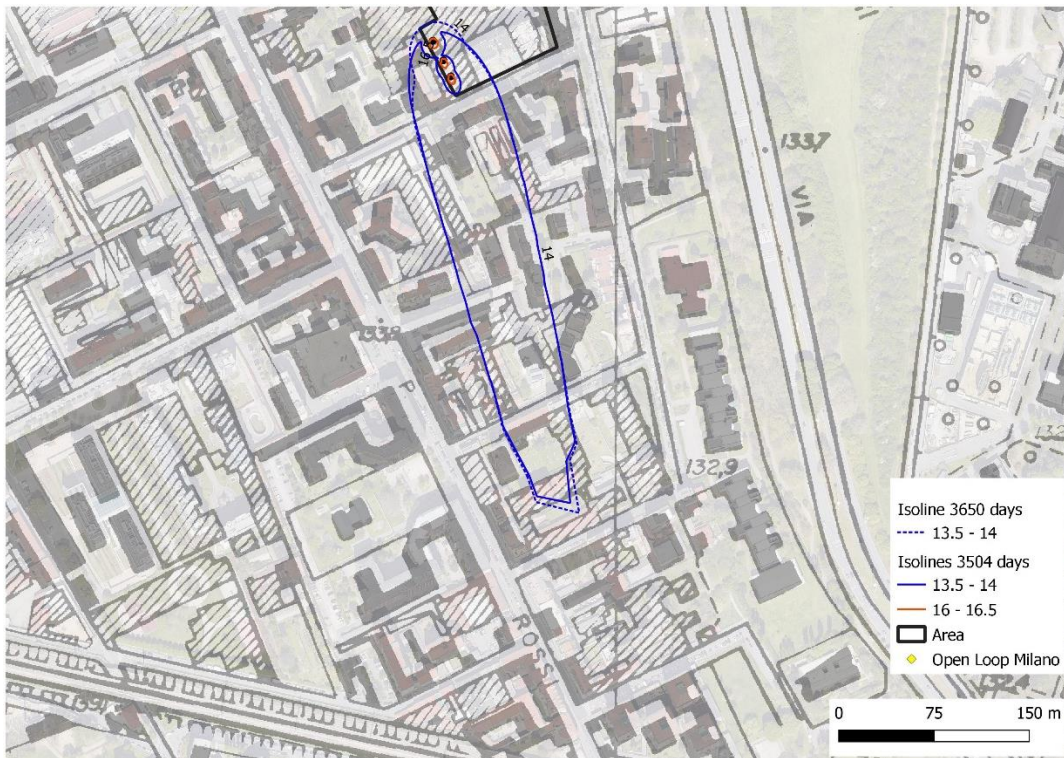


Fig. 62. Isolines 14 °C at 10 years.

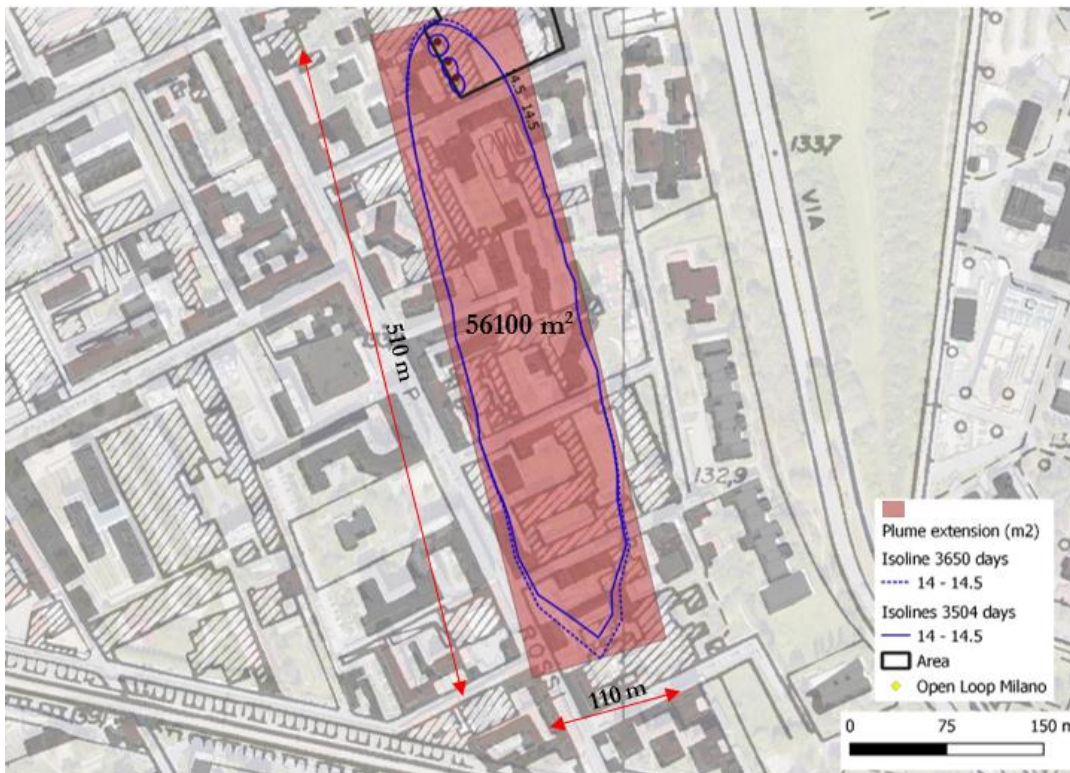


Fig. 63. Thermal plume extension.

The simulation was extended till 50 years, respectively to 18 104 days in Fig. 64 and Fig. 65 (cooling mode) and 18250 days (heating mode) in Fig. 66 and Fig. 67.





Fig. 64. Thermal plume after 18'104 (cooling mode).

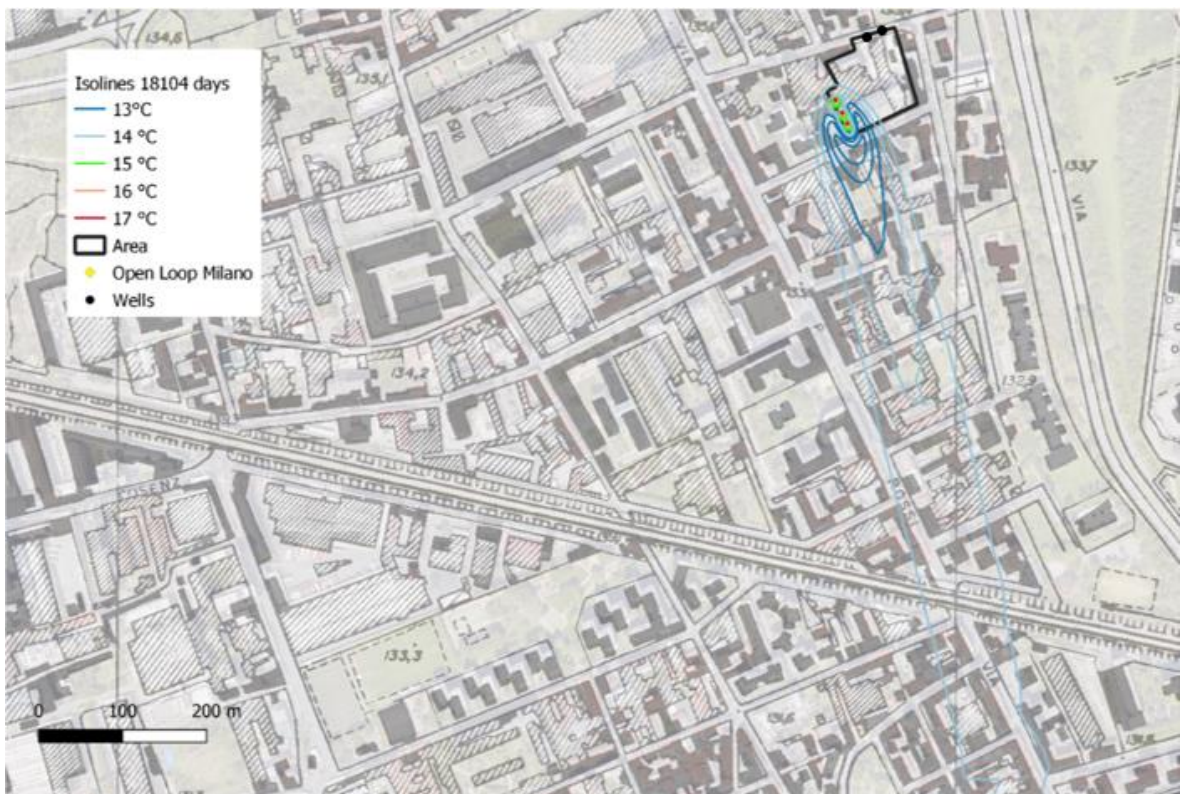


Fig. 65. Detail of thermal plume after 18'104 days.



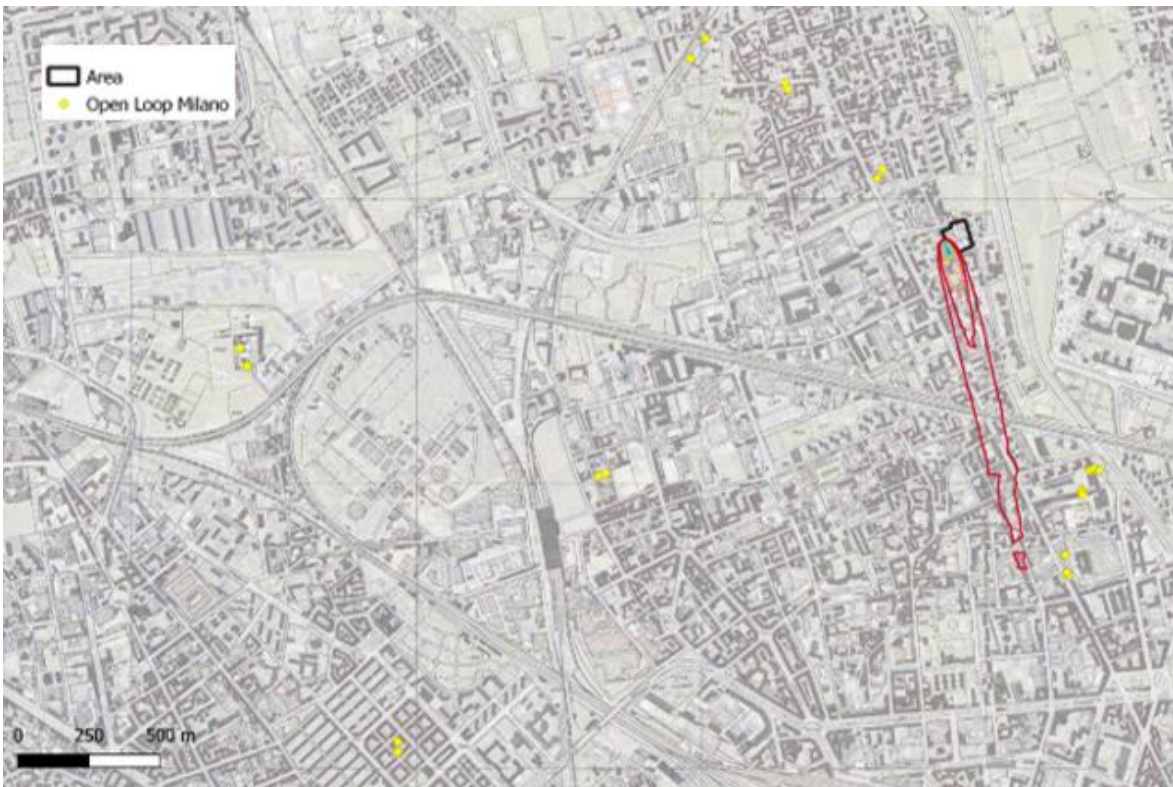


Fig. 66. Thermal plume after 18'250 days (heating mode).

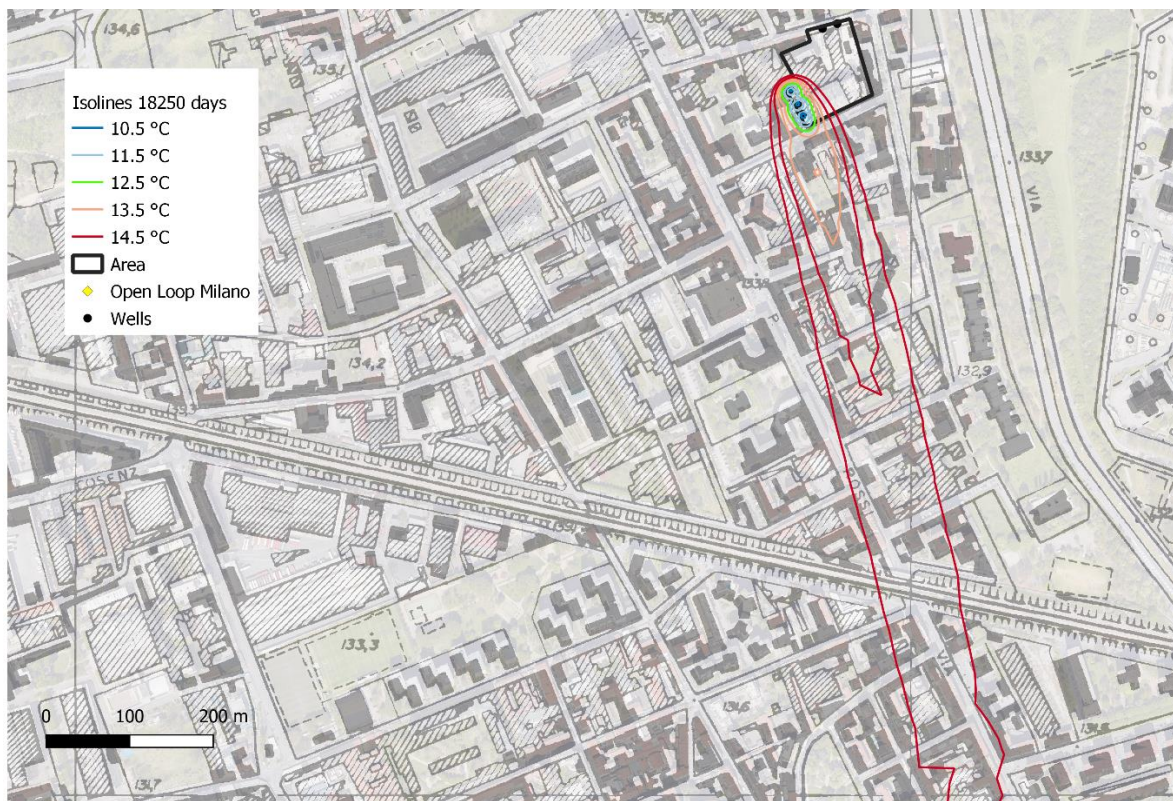


Fig. 67. Detail thermal plume after 18'250 days.

In Fig. 68 the diagram of local temperatures recorded by the observation existing wells distributed on the area of Milan. The local temperature trend result function of development time of plume and observation wells position. In particular, can be affirm that around 50 years is reached the steady state condition of temperature for each well, result of an equilibrium condition developed between injection water and groundwater; moreover, the relevant variations of temperature are recorded around the injection wells due to the operating cycle of the plant.

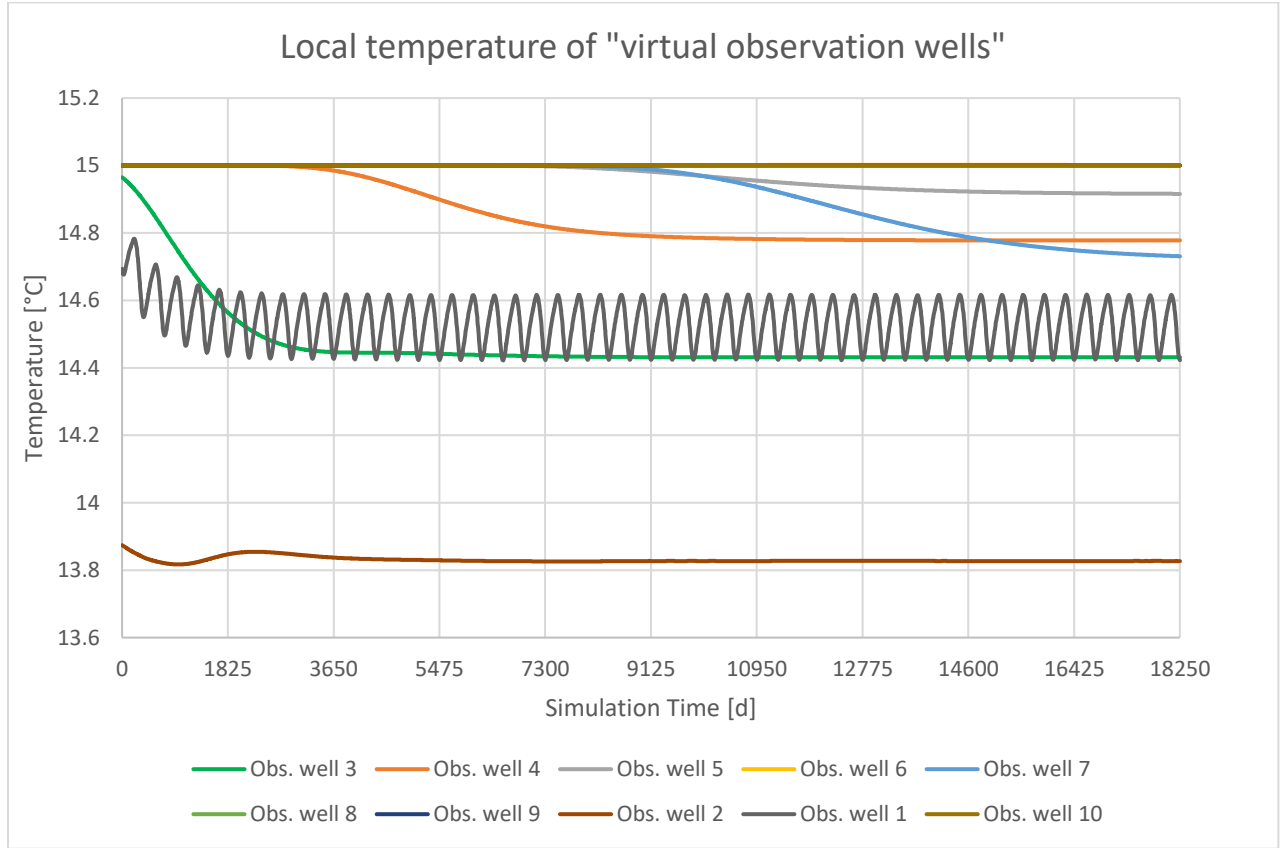


Fig. 68. Local temperature variation recorded by observation wells.

Focusing the attention on the isolines 14 °C, corresponding to the variation of 1°C compared to the equilibrium temperature state fixed at 15°C of aquifer, the thermal plume at 10 and 50 years coincide, as is possible see in Fig. 69. This result confirms how the temperature alteration of groundwater reached an equilibrium state just after 10 years. The impact of thermal plume results limited at that area, where is originated a dynamic equilibrium between injection fluid and groundwater, between which is established a temperature deficit compensate by the irradiation of sun according to the thermodynamic principle. However, the area affected by thermal plume is low entities as shown in Fig. 70.



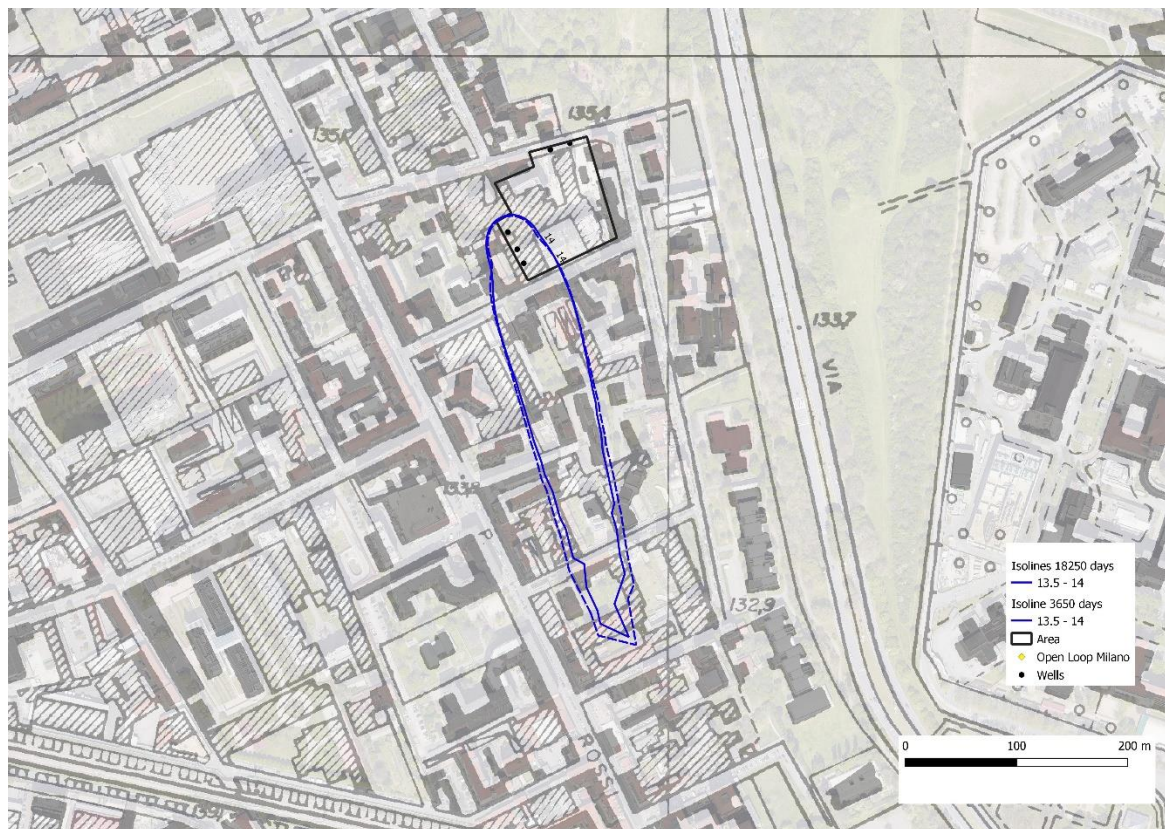


Fig. 69. Isolines 14°C: 10 years vs 50 years.

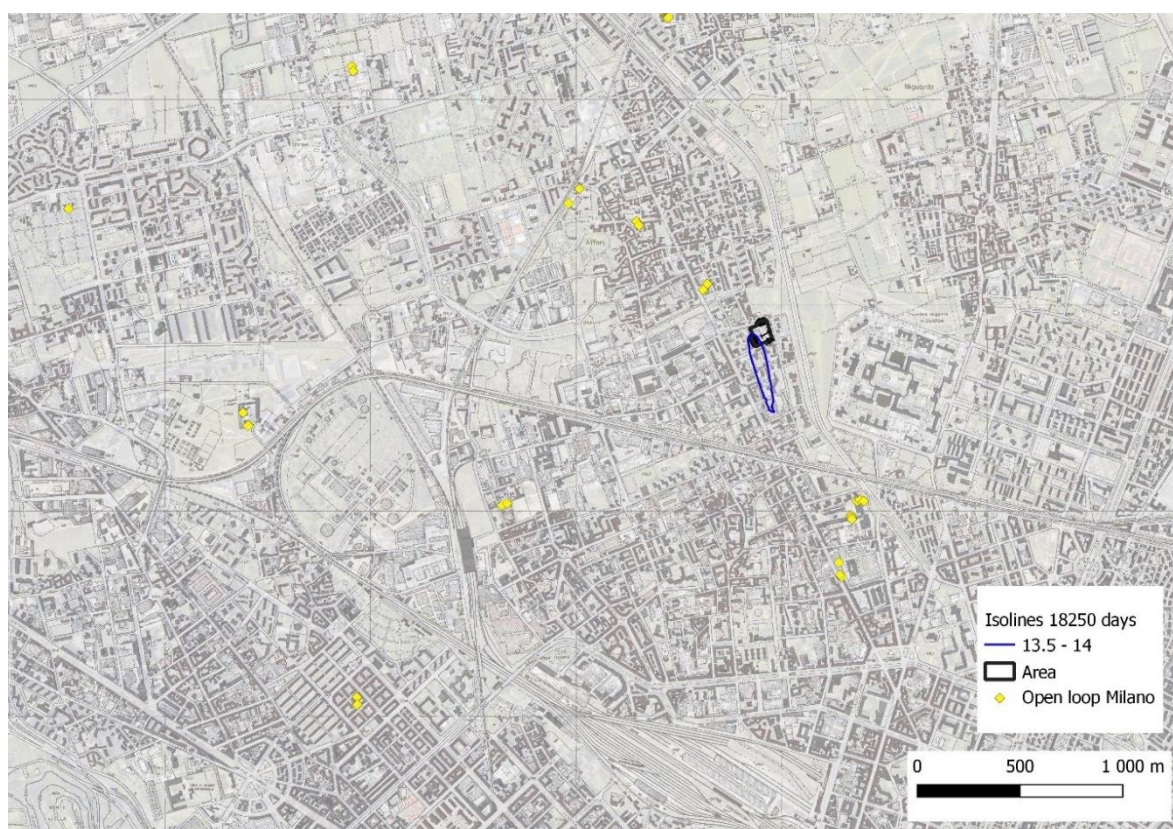


Fig. 70. Impact isolines 14 °C on total area.

## 5 CONCLUSIONS

In prevision of an increasingly green future based on the development and exploitation of renewable resources, shallow geothermal systems result to be one of the most suitable and least invasive solution regard energy efficiency comparts.

The project “Residenza Parco delle Favole” located in Via Pastro 22 in Milan is a representative example of new building, aimed to exploit the natural resource without environmental impact. The shallow geothermal system designed based on a system of wells for the extraction of groundwater, which, following the exchange whit heat pump of thermal energy, is consequently injected through three injection wells placed downstream in the aquifer.

The heat pumps installed in the respective thermal power stations, for heating, cooling, and hot domestic purposes, operating in in two moods controlled by thermal load, deduced from the energy need studies of 100 civil units distributed in three building.

In order to evaluate the environmental impacts of this geothermal plant, the examined area was modelled using finite element numerical code FEFLOW 7.5. The area was reconstructed from hydrogeological and morphological point of view, an evaluation enhanced by the installed monitoring network whose data provided further information on the state of the water resource, in order to obtain reliable results. In the same way, all the inputs concerning the operating cycle of the shallow open loop geothermal system have been set. This made it possible to carry out a simulation of heat flow and transport, studying the development of the thermal plume and its impact on the water resource. The simulation was extended at regular intervals of 30.5 days for a total duration of 10 years at the end of which the impact of the plumes was assessed with respect to the equilibrium temperature, set at 15° C. The greatest temperature gradients occur closer to the injection wells.

The analysis on the possible sustainable installation density of these types of systems in the area of Milan, the simulation was extended till 50 years. The evaluation was focused on the isolines 14°C, corresponding to 1°C alteration of groundwater temperature. The plume invests an area equal to 5.6 ha of low entities and not involved any other existing geothermal plant installed. Moreover, the results attest how the steady state condition was just reached at 10 years, results of an equilibrium state condition established between aquifer, geothermal plant. Further results concern the absence of any thermal recirculation phenomenon, common for this type of systems that compromise the maximization of system efficiency.

In conclusion, open loop systems such as the one analysed are the right energy efficiency alternative in perfect agreement with the policy we are experiencing of decarbonisation and environmental protection

## REFERENCES

- [1] ENEA, Rapporto Annuale Efficienza Energetica, (2021). <https://bit.ly/3fdTYwb> (accessed September 23, 2022).
- [2] S.J. Self, B.V. Reddy, M.A. Rosen, Geothermal heat pump systems: Status review and comparison with other heating options, *Applied Energy*. 101 (2013) 341–348. <https://doi.org/10.1016/j.apenergy.2012.01.048>.
- [3] Repubblica Italiana, D.Lgs. 22/2010 - Riassetto della normativa in materia di ricerca e coltivazione delle risorse geotermiche, a norma dell'articolo 27, comma 28, della legge 23 luglio 2009, n. 99 (Legislative decree 22/2010 - Reorganization of legislation on survey and exploitation of geothermal resources), (2010). <http://www.camera.it/parlam/leggi/deleghe/10022dl.htm> (accessed January 4, 2019).
- [4] Tecnologia e potenzialità dei sistemi geotermici a bassa entalpia - Alessandro Casasso, Rajandrea Sethi. Aprile 2013.
- [5] Hydraulic Down the Hole Drilling. <https://hartrusion.com/en/hydrdthhammer/>. <https://hartrusion.com/en/hydrdthhammer/>.
- [6] Water Wells and Boreholes-Bruce Misstear, David Banks, Lewis Clark. <https://bit.ly/3fRxb9F>.
- [7] M. Caleffi, F. Guidetti, S. Casarino, A. Crimella, M. Doninelli, D. Mazzetti, R. Planca, A. Soldarini, C. Tadini, M. Tadini, M. Tomasoni, Impianti a pompe di calore geotermiche, 2010.
- [8] Urbanfile Blog, Milano Affori - Le Residenze Parco delle Favole, (2021). <https://bit.ly/3R7FE2m> (accessed September 23, 2022).
- [9] Carta Geologica d'Italia, Milano- Foglio118. <https://bit.ly/3C6tnJb>.
- [10] Relazione Illustrativa delle Componenti Geologica, Idrogeologica e Sismica (PGT) Comune di Milano -<https://bit.ly/3r6VkJL>.
- [11] Alpha innotect product- Heat pumps- <https://bit.ly/3FaRgT0>.
- [12] Tubi in u-pvc per pozzi- GTS well components - <https://bit.ly/3BW0KOM>.
- [13] Ingegneria degli acquiferi - Antonio Di Molfetta, Rajandrea Sethi-Springer-Verlag Italia 2012.
- [14] Geotru software - <https://bit.ly/3C7XfF7>.
- [15] Levellogger 5 Water Level Dataloggers- Solinst.<https://bit.ly/3MbnQWo>.
- [16] Surface Level meter-Sonlist. <https://bit.ly/3M8dDd5>.
- [17] Ultrasonic Flow Meter User Manual-Type: TUF-2000B.